Nature Communications

https://doi.org/10.1038/s41467-026-75618-0

Article in Press

Rice PROTEIN L-ISOASPARTYL METHYLTRANSFERASES provides tolerance against sheath blight disease and repairs ALDH and PBZ1

Received: 13 January 2026

Accepted: 1 July 2026

Published online: 21 July 2026

Cite this article as: Gautam, S., Kamble, N.U., Achary, R.K. *et al.* Rice PROTEIN L-ISOASPARTYL METHYLTRANSFERASES provides tolerance against sheath blight disease and repairs ALDH and PBZ1. *Nat Commun* (2026). https://doi.org/10.1038/s41467-026-75618-0

Shikha Gautam, Nitin Uttam Kamble, Rakesh Kumar Achary, Ravindra Kumar Chandan, Vishal Varshney, Abhijit Hazra, Saroj Laha, Shivangi Mahawar, Sohela Mehandiratta, Sarvanand Singh, Gopaljee Jha & Manoj Majee

Rice PROTEIN L-ISOASPARTYL METHYLTRANSFERASES provides tolerance against sheath blight disease and repairs ALDH and PBZ1.

Shikha Gautam[#1], Nitin Uttam Kamble[#1,2], Rakesh Kumar Achary[1], Ravindra Kumar Chandan[1], Vishal Varshney[1], Abhijit Hazra[1], Saroj Laha[1], Shivangi Mahawar[1], Sohela Mehandiratta[1], Sarvanand Singh[1], Gopaljee Jha[1]* and Manoj Majee[1]*

# Authors contributed equally *Corresponding authors

[1]. BRIC-National Institute of Plant Genome Research (NIPGR), Aruna Asaf Ali Marg, New Delhi 110067, India.

[2]. School of Biology, Indian Institute of Science Education and Research, Thiruvananthapuram, India.

Corresponding authors:

manojmajee@nipgr.ac.in

jmsgopal@nipgr.ac.in

Abstract

Protein L-isoaspartyl methyltransferase (PIMT) regulates key seed traits and abiotic stress tolerance in plants by repairing isoaspartyl (isoAsp) damaged proteins. However, whether PIMT-mediated repair is induced and is required during biotic stress tolerance remains unknown. Using rice lines with OsPIMT overexpression, RNAi-mediated suppression, and genome editing, we show that PIMT enhances tolerance to sheath blight (ShB) caused by *Rhizoctonia solani*. OsPIMT restricts fungal penetration and colonization of rice sheaths. Co-immunoprecipitation coupled with LC-MS/MS identify various proteins including antioxidant proteins, aldehyde dehydrogenases (ALDH) and pathogenesis-related protein 10 (PBZ1), that undergo isoAsp modification during *R. solani* infection and interact with PIMT. We show that OsALDH

and OsPBZ1 exhibit intrinsic antifungal activity against *R. solani*, but isoAsp modification impairs their activity, making PIMT mediated repair important. Further, OsALDH enhances tolerance to *R. solani* by inhibiting lipid peroxidation and ROS homeostasis in rice and fungus. Overall, our study reveals that PIMT enhances ShB tolerance through the repair of isoAsp-damaged proteins important for disease tolerance.

Introduction

Rice (*Oryza sativa*) serves as a fundamental dietary component for the majority of the population worldwide; therefore, ensuring consistent and robust rice yield is crucial for global food security. Sheath blight disease (ShB) caused by the necrotrophic fungus *Rhizoctonia solani Kuhn* (*R. solani*), poses a major threat for rice cultivation worldwide[1]. *R. solani* can infect rice at any developmental stage, reducing yield by over 50%, hence severely compromising yield and production stability[2].

The dynamic interaction between plant pathogens and the host immune system involves counter-defense strategies deployed by both sides. Among many of these mechanisms, Reactive Oxygen Species (ROS) plays a central role in immune responses, regulated through a balance of ROS production and detoxification[3,4]. However, this finely-tuned homeostasis is compromised under various abiotic and biotic stresses, leading to excessive ROS accumulation, which often instigates and promotes oxidative cell death[5]. In defense, ROS plays a dual role, triggering plant's basal defense response with biotrophic and hemibiotrophic pathogens while inducing susceptibility against necrotrophs. For instance, downregulation of peroxidases III (*OsPrx30)*, a ROS-scavenging gene, enhances resistance against bacterial blight[6]. Contrastingly, overexpression of *OsPrx114*, another peroxidase family gene, significantly enhances resistance to *Sclerotinia sclerotiorum* and *Botyrtis cinerea* by rapidly scavenging ROS leading to enhanced lignin formation[7,8]. Moreover, ShB-resistant rice genotypes show an abundance of antioxidant enzymes, implying the importance of ROS homeostasis in modulating resistance to ShB[9]. *R. solani* infection elevates

ROS levels and induces host cell death[10,11] hence balance of ROS is critically needed in ShB resistance. However, merely scavenging ROS may be insufficient to enhance host defense response, and additional enzymes or functions are needed.

Lamentably, excessive ROS accumulation is known to cause damage in DNA, RNA, and proteins[12]. Proteins, however, are inherently vulnerable to structural and functional damage during stress. Proteins accumulate spontaneous modifications, such as isoAsp formation, methionine oxidation, etc., compromising the protein's structure and biological function[13,14]. These detrimental modifications are recognized and reversed by protein-repairing mechanisms. Among these, protein repairing enzyme PROTEIN L-ISOASPARTYL METHYLTRANSFERASES (PRE-PIMT), specifically recognizes L-isoaspartate (isoAsp) residues in proteins and transfers a methyl group from AdoMet to carboxyl group of L-isoAsp, recovering protein's functionality[15,16].

The detrimental effect of isoAsp formation and the function of PIMT in orthodox seeds have been thoroughly investigated and shown to be involved in maintaining seed vigor and longevity[16-24]. During seed maturation, PIMT expression is modulated by ABA and ABI transcription factors, contributing to desiccation tolerance and seed lifespan in orthodox seeds of *O. sativa*, but not in the recalcitrant seeds of *O. coarctata*[22,26]. Recent reports have also suggested PIMT's role in improving seed agronomic traits in rice by repairing enolases, PABPs and HSFs (Heat Shock Factor)[24,25,27].

Apart from seeds, PIMT has been reported to promote growth and stress tolerance by modulating ROS homeostasis under abiotic stresses such as heat, oxidative and salt stress in Arabidopsis. This stress tolerance is attained by repairing antioxidative enzymes CATALASE (CAT) and SUPEROXIDE DISMUTASE (SOD) from isoAsp-mediated protein damage[26,28,29]. Several such substrate proteins of PIMT have also been identified in many plant species[24,27,29-31]. Although, PIMT's role has been well explored in seed and abiotic stress tolerance, yet its specific involvement in the plant defence against pathogens (bacterial or fungal) has not been elucidated. Furthermore, isoAsp-mediated protein damage and its possible

adverse effects during plant diseases remain elusive. Here, we demonstrated that PIMT positively influences tolerance against rice ShB disease caused by *R. solani*. We identify proteins including, antioxidative proteins, aldehyde dehydrogenases (ALDH) and pathogenesis related 10 protein (PBZ1) that undergo isoAsp modification, affecting their biological functions, upon *Rhizoctonia* infection. We further show that OsALDH limits infection by suppressing lipid peroxidation and maintaining ROS homeostasis in both rice and the pathogen. Our data also suggests that OsALDH and OsPBZ1 also possess intrinsic antifungal activity against *R. solani*.

Results

isoAsp accumulation and PIMT activity increase during *R. solani* infection in rice

To understand the extent of ROS and subsequent isoAsp-mediated protein damage, as well as the role of protein repair by the PIMT enzyme and their combined effects on biotic stress tolerance, we examined isoAsp and ROS accumulation in rice sheaths at different days post-inoculation (dpi) during *R. solani* infection. A gradual increase in ROS accumulation from 1 to 4 dpi was revealed by DAB (3,3′-diaminobenzidine) and NBT (Nitro Blue Tetrazolium) staining. This increase in ROS levels led to cell death, as visualized by TB (Trypan Blue) staining, consistent with the elevated ROS accumulation (Fig. 1a). We observed that increased ROS accumulation induces protein damage as infection progresses, quantified as total isoAsp accumulation (Fig. 1b). Next, to analyse whether this increased isoAsp induces PIMT to counter such high isoAsp content during infection, we quantified total PIMT activity. Our analysis reveals PIMT activity progressively increased till 3dpi and then stayed similar to uninfected control tissues (Fig. 1c). Next, we analysed transcript and protein accumulation of *OsPIMT1* and *OsPIMT2*. *OsPIMT1* transcript and protein accumulation followed a pattern consistent with total PIMT activity, however the expression levels of *OsPIMT2* remain unaltered at earlier time points and is reduced at later time points (Fig. 1e). In accordance with our previous study[21], these findings clearly indicate that *OsPIMT1* and *OsPIMT2* exhibit distinct and tissue-specific expression patterns: OsPIMT1 is the predominant isoform in

vegetative tissues, including rice sheaths, whereas both isoforms contribute to seed development. Western blot (WB) analysis also confirmed an increase in OsPIMT1 protein level upon *R. solani* infection (Fig. 1f). Collectively, these results confirm that isoAsp accumulation occurs during infection, leading to the induction of PIMT activity and suggest a potential role for PIMT, specifically *OsPIMT1* in the response to *R. solani*. Plant hormones are vital players in plant immunity. Given the necrotrophic nature of the pathogen; tolerance to *R. solani* is expected to be JA-dependent[31]. Therefore, to analyse total JA and SA contents upon *R. solani* infection, we performed hormone quantification. In accordance with the previous reports, we observed increased JA accumulation in WT plants upon *R. solani* infection, while SA content was reduced (Supplementary Fig. 1a, b). Since, JA content is increased nearly 3.5-fold, we investigated whether the enhanced *OsPIMT1* expression observed in Fig. 1d was JA dependent, and whether JA alone could induce the expression of *OsPIMTs.* Analysis of expression patterns of *OsPIMTs*, PIMT activity and protein accumulation in WT seedlings following JA treatment at different time-points confirmed that *OsPIMTs* transcript accumulation, as well as PIMT activity and protein accumulation is indeed induced upon exogenous JA application. However, in both *R. solani* infection and JA treatment conditions *OsPIMT1* showed the highest induction, whereas *OsPIMT2* was induced only in response to JA treatment (Supplementary Fig. 1c-f).

***OsPIMTs* enhance tolerance against *R. solani* infection and restricts fungal penetration**

As shown in Fig. 1, we observed that increased PIMT activity is required to restrict isoAsp accumulation upon *R. solani* infection. Therefore, to genetically investigate the role of *OsPIMTs* in *R. solani* pathogenesis, we characterized our previously generated and confirmed transgenic rice lines constitutively overexpressing (*OE*) either *OsPIMT1* (*OsPIMT1:OE*) or *OsPIMT2* (*OsPIMT2:OE*), alongside *OsPIMTs*-RNAi (*OsPIMT:RNAi*) knockdown (targeting both *OsPIMT1* and *OsPIMT2*) lines[21,22]. WT, along with all these lines, were evaluated at 3dpi for their defense response upon *R. solani* infection. Compared with WT, *OsPIMT1:OE* and *OsPIMT2:OE* lines showed significantly enhanced tolerance (Fig. 2a). Notably, *OsPIMT:RNAi* lines were more susceptible to *R. solani* infection, producing an increased number of lesions

with larger size. This distinct response was further demonstrated by Relative Vertical Sheath Colonization (RVSC), revealing significant differences in *R. solani* tolerance among these lines (Fig. 2b, c). Next, we investigated the impact of *PIMT* overexpression and knockdown on *R. solani* infection, evaluating the pathogen load, quantifying *Rs18S rRNA* expression as fungal biomass via RT-qPCR, in infected sheaths. Low pathogen load was present in both *OsPIMT1:OE* and *OsPIMT2:OE* lines in contrast to elevated levels in *OsPIMT:RNAi* lines and WT plants (Fig. 2d). To further validate the role of PIMT in enhancing tolerance against *R. solani*, we extended our analyses up to 6dpi and observed enhanced tolerance in case of OE lines while *PIMT RNAi* lines were more susceptible compared to the WT similar to infection phenotypes observed at 3dpi (Supplementary Fig. 2).

Given the critical role of host penetration in governing successful fungal pathogen colonization and disease establishment[32], we proceeded to analyse *R. solani* colonization patterns within infected rice sheaths. Since, the infection phenotypes were similar in both 3dpi and 6dpi we utilized samples of 3dpi for further analyses. Confocal microscopy, with WGA-FITC staining, demonstrates restricted penetration depth in *OsPIMT:OE* lines. However, extensive hyphal penetration was observed in infected sheaths of WT and *RNAi* lines (Supplementary Fig. 3). Furthermore, 3D topological imaging reinforced these findings, depicting a dense mycelial mat in WT and *OsPIMT:RNAi* lines, while *OsPIMT:OE* lines showed scattered minimal fungal growth (Fig. 2e), further validated by fungal penetration depth plot (Fig. 2f).

To establish the relationship among PIMT, isoAsp accumulation and *R. solani* tolerance, isoAsp accumulation was quantified in *OsPIMT:OE, OsPIMT:RNAi* and WT plants with and without infection of *R. solani*. Upon infection, increased levels of isoAsp were detected in all genotypes; however, the degree of elevation of isoAsp content significantly differed among *OsPIMT:OE, OsPIMT:RNAi* and WT plants. RNAi lines, which had reduced PIMT activity, exhibit increased accumulation of isoAsp relative to the WT plants. In contrast, *OsPIMT:OE* lines with increased PIMT activity had significantly reduced isoAsp content than that of the WT and *OsPIMT:RNAi* plants (Fig. 2g). These results provide evidence that PIMT

activity is important to reduce *R. solani* induced isoAsp accumulation and thereby restrict *R. solani* infection.

Next, we examined the transcript levels of several defense-related genes in response *R. solani* infection[33,34], such as the *pathogenesis-related (PR) gene, PR5 (a thaumatin-like protein gene),* and JA-related genes, *LOX (lipoxygenase), AOS (allene oxide synthase), GSL5 (Callose synthase)* and *AOC (allene oxide cyclase).* The results demonstrated that *PR5*, *LOX*, *AOS*, and *AOC* were evidently elevated in the *OsPIMT*:*OE* lines compared with WT plants. On the contrary, their expression was remarkably decreased in the *OsPIMT:RNAi* lines (Supplementary Fig. 4). Taken together, these findings demonstrate that *PIMT* overexpression compromises *R. solani's* capacity for effective host colonization and penetration, providing tolerance to ShB.

_OsPIMT_s restricts ROS accumulation and cell death during _R. solani_ infection

ROS accumulation is one of the early responses during the *R. solani* infection, which follows a brief biotrophic phase followed by a necrotrophic phase[35,36]. ROS accumulation induces cell death, that favour colonization and growth of *R. solani*. Therefore, ROS balance is needed to mount defense against *R. solani* infection. To determine if the compromised *R. solani's* colonization and penetration in *OsPIMT*:*OE* lines was linked to ROS homeostasis, we visualized cellular ROS accumulation by H_2DCFDA staining using confocal microscope and observed lesser ROS accumulation in *OsPIMT*:*OE* lines compared to the WT and *OsPIMT:RNAi* lines (Fig. 3a). We then performed DAB and TB staining that confirms reduced ROS accumulation which in turn reduces cell death in *OsPIMT*:*OE* lines compared to WT and *OsPIMT:RNAi* lines (Fig. 3b). We quantified the accumulation of H_2O_2, which validated less ROS accumulation in *OsPIMT*:*OE* lines as compared to WT and *OsPIMT:RNAi* lines (Fig. 3c). In continuation of reduced cell death, we also observed significantly reduced levels of MDA in *OsPIMT*:*OE* lines as compared to WT and *OsPIMT:RNAi* lines (Fig. 3d), depicting less cellular damage to the cell wall due to lipid peroxidation[37,38] further supporting reduced cell death and improved cell wall strength. Next, we investigated the activity of antioxidative enzymes, which are known to be susceptible to isoAsp modification under abiotic stress[27-28,

in these genotypes. We observed that *OsPIMT:OE* lines maintained substantially higher Ascorbate Peroxidase (APX) and Catalase (CAT) activity compared to the WT and *OsPIMT:RNAi* lines upon *R. solani* infection (Fig. 3e, f). In contrast, the activities of these enzymes remained largely unchanged under control conditions (Supplementary Fig. 5 a, b). Taken together, these analyses confirmed that PIMT plays a key role in limiting ROS accumulation and maintaining antioxidative enzymes activity during *R. solani* infection.

pimt mutants exhibit hyper susceptibility to _R. solani_ infection, accumulate more ROS and isoAsp, and show increased cell death

To further confirm PIMT's role in conferring ShB disease tolerance in rice, we generated genome-edited lines of *PIMTs* using CRISPR/Cas9. Successful generation of multiple genome-edited lines was confirmed by sanger sequencing (Fig. 4a, b; Supplementary Fig. 6 a, b). Overall, *pimt1* mutant plants exhibited a significant reduction in growth parameters and PIMT enzymatic activity compared with WT plants. In contrast, *pimt2* mutant plants did not show any significant differences in growth parameters or PIMT activity relative to WT plants again reinforcing the tissue specific expression of *PIMT*s (Supplementary Fig. 7).

WT and all mutant lines were subsequently evaluated at 3dpi for their defence responses against *R. solani* infection. The *pimt1* mutant lines displayed severe disease symptoms compared with WT plants (Fig. 4c; Supplementary Fig. 8), which was supported by increased RVSC (Fig. 4d) and significantly longer lesion lengths (Fig. 4e). Although infection led to elevated isoAsp accumulation in all genotypes, the increase was significantly greater in *pimt1* mutant plants (Fig. 4f). Disease symptoms were also observed in *pimt2* mutant lines; however, they were less severe as compared to *pimt1* mutant plants (Fig. 4). These findings indicate that reduced PIMT activity and enhanced isoAsp accumulation contribute to increased disease susceptibility in rice. To further validate the persisting susceptibility against *R. solani* of these genome editing lines, we extended our analyses up to 6dpi and observed persistent susceptivity and vigorous infection in genome edited lines particularly *pimt1* mutants (Supplementary Fig. 9).

Next, we analysed pathogen load and performed WGA-FITC staining coupled with 3D imaging, as conducted for the *OsPIMT:OE* and *OsPIMT:RNAi* lines. Compared with WT plants, the mutant lines exhibited a significantly higher pathogen load, accompanied by extensive fungal penetration and the formation of dense mycelial mats (Fig. 4g-i; Supplementary Fig. 10).

To further investigate the physiological basis underlying the enhanced susceptibility of the *pimt* mutant lines, we examined ROS accumulation, cell death, antioxidative enzyme activities, and defense-related hormone responses following *R. solani* infection. The mutant lines showed substantially greater ROS accumulation, as evidenced by H_2DCFDA, DAB and TB staining, along with increased cell death and higher MDA content compared with WT plants (Fig. 5a-d). In addition, analysis of antioxidative enzyme activities revealed significantly reduced APX and CAT activities in the *pimt* mutant lines following infection (Fig. 5e, f), whereas these activities remained largely unchanged under control conditions (Supplementary Fig. 11a, b).

Because jasmonic acid (JA)-mediated signaling plays a central role in defense against necrotrophic pathogens, we next performed hormone profiling and analyzed the expression of defense-related genes. Notably, *pimt* mutants accumulated lower JA levels and exhibited downregulation of JA-responsive defense genes compared with WT plants, which likely contributes to their enhanced susceptibility to *R. solani* (Supplementary Fig. 12a-c).

Collectively, these findings reinforce our conclusion that PIMT plays a critical role in restricting ROS accumulation, maintaining antioxidative enzyme activity, and sustaining JA-mediated defense responses during *R. solani* infection, thereby contributing to enhanced disease tolerance in rice.

PIMT maintains OsALDH and OsPBZ1 function following isoAsp modification during *R. solani* infection

To elucidate the mechanisms underlying PIMT-mediated tolerance, we sought to identify potential interacting partners and substrate proteins of PIMT during *R. solani* infection. To do this, we performed an

unbiased immunoprecipitation assay using total protein extracts from infected WT rice sheaths with an anti-PIMT antibody, followed by LC-MS/MS analysis to identify OsPIMT-associated proteins.

The analysis identified several antioxidative proteins, including CAT, APX, and SOD, along with aldehyde dehydrogenase OsALDH7 (*LOC_Os09g26880*) and the pathogenesis-related protein OsPBZ1/OsPR10a (*LOC_Os12g36880*), among many other potential OsPIMT-interacting proteins in response to *R. solani* infection (Supplementary Table 1). The identification of antioxidative proteins such as CAT, SOD, and APX further strengthened the reliability of our IP-MS/MS analysis, as our previous studies demonstrated that these proteins interact with PIMT and also serve as its substrate proteins[25,28].

Importantly, tryptic peptides of CAT, APX, OsALDH7 and OsPBZ1 identified through IP-MS/MS analysis exhibited deamidation at specific asparagine residues, including N^{72} in CAT, N^{391} in APX, N^{458} in OsALDH7 and N^{57} in OsPBZ1 (Fig. 6e, f; Supplementary Fig. 13).

Given our earlier findings that PIMT repairs stress-induced isoAsp accumulation in OsAPX [26], we next examined isoAsp accumulation in immunoprecipitated APX using anti-APX antibodies from WT and *pimt1* plants infected with *R. solani*. Our results revealed increased isoAsp accumulation in immunoprecipitated APX pulled from *pimt1* plants compared with the WT plants (Supplementary Fig. 13c). These findings indicate that these proteins undergo isoAsp modification during *R. solani* infection. To further investigate the prevalence of such modifications, we analyzed the sequences of rice ALDH and PBZ family proteins for potential asparagine (Asn) and aspartate (Asp) residues susceptible to isoAsp formation. Sequence analysis revealed that all members of both protein families contained at least one residue highly susceptible to isoAsp formation (Supplementary Table 2).

Expression profiling using publicly available databases further showed that most OsALDH family members are expressed in leaves or sheaths; however, only *LOC_Os09g26880* and *LOC_Os02g49720* displayed strong induction upon pathogen infection (Supplementary Fig. 14). Similarly, OsPBZ1 (*LOC_Os12g36880*) exhibited high expression in leaves and sheaths and was strongly induced during pathogen infection (Supplementary Fig. 15).

In our previous study[25], we identified *At1g54100* (Aldehyde Dehydrogenase 7B4), the Arabidopsis homolog of *LOC_Os09g26880*, as a PIMT-interacting protein. Based on these observations, we selected *LOC_Os09g26880* (hereafter referred to as OsALDH) and *LOC_Os12g36880* (hereafter referred to as OsPBZ1) for detailed molecular and biochemical analyses. These candidates were prioritized because of both their mechanistic significance and their established biological functions: OsALDH is involved in aldehyde detoxification, ROS homeostasis, and mitigation of lipid peroxidation[39,40], whereas OsPBZ1 possesses RNase activity associated with broad-spectrum disease resistance[41,42]. Thus, our focus on OsALDH and OsPBZ1 builds upon established ROS-isoAsp-PIMT regulatory framework while extending it to defense-associated targets.

Given that LC-MS/MS analysis revealed isoAsp modifications in these proteins, we next investigated whether oxidative stress could directly induce such modifications *in-vitro*. To do this purified recombinant OsALDH and OsPBZ1 proteins (Fig. 6a, b) were exposed to 30mM H_2O_2 at 25°C, followed by quantification of isoAsp accumulation. Interestingly, H_2O_2-treated proteins exhibited significantly higher isoAsp levels compared with untreated controls (Fig. 6c, d). Subsequent MS/MS analyses further confirmed deamidation at several asparagine residues [OsALDH: N^{136} and N^{458}; OsPBZ1:N^{45} and N^{57}] in the H_2O_2-treated proteins (Supplementary Fig. 16 and 17; Supplementary Dataset 1). Notably, N^{45} lies in the active site motif of OsPBZ1, suggesting that such modifications could directly impair protein function. Together, these *in-vivo* and *in-vitro* analyses demonstrate that elevated ROS levels may trigger isoAsp formation in both native and purified proteins.

To determine whether isoAsp accumulation negatively affects protein function and whether OsPIMT can repair these stress-induced modifications, we performed *in-vitro* PIMT repair assays using purified recombinant OsPIMT1 (catalytically active) or (catalytically inactive) OcPIMT1-2 serves as negative control in reaction (does not have any PIMT activity)[22] in the presence of the methyl donor AdoMet and H_2O_2-treated OsALDH or OsPBZ1 proteins. In our previous work, we have identified a PIMT isoform OcPIMT1-2 from wild rice (*Oryza coarctata*) which is biochemically inactive due to the lack of a conserve

motif (Region II) of PIMT protein required for PIMT activity[22]. A significant reduction in isoAsp content was observed in both OsALDH and OsPBZ1 when catalytically active OsPIMT1 was included in the reaction, whereas no such reduction was observed with inactive OcPIMT1-2 (Fig. 6g, h). These findings suggested that ROS induced isoAsp accumulation may compromise the catalytic efficiency of OsALDH and OsPBZ1, which can subsequently be restored by PIMT-mediated repair.

To further evaluate functional recovery, we performed enzymatic activity assays for OsALDH and OsPBZ1. OsALDH activity assays were conducted according to Tsuji et al.,[43] with minor modifications using protein extracts from bacterial cells expressing recombinant OsALDH. IPTG-induced cells displayed enhanced OsALDH activity relative to uninduced controls. However, treatment of IPTG induced extracts with H_2O_2 significantly reduced enzymatic activity, indicating stress-induced functional impairment likely associated with isoAsp accumulation. Remarkably, supplementation with OsPIMT1 and AdoMet restored OsALDH activity, whereas inactive OcPIMT1-2 failed to confer this recovery (Fig. 6i).

Similarly, RNase activity assays performed with recombinant OsPBZ1 demonstrated that H_2O_2 treatment substantially reduced its enzymatic activity. Importantly, this loss of activity was effectively restored upon addition of active OsPIMT1, while inactive OcPIMT1-2 was unable to restore enzyme function (Fig. 6j). Collectively, these results demonstrate that OsPIMT1 could maintain the enzymatic activities of OsALDH and OsPBZ1 under oxidative stress by repairing isoAsp-mediated protein damage

OsPIMTs physically interact with OsALDH and OsPBZ1

As shown in Fig. 6, both OsALDH and OsPBZ1 underwent isoAsp modifications following *R. solani* infection and H_2O_2 treatment. Since PIMT mediates repair through direct interaction with its substrate proteins, we next sought to determine whether OsPIMTs physically interact with these target proteins. Initially, the subcellular localization of transiently expressed OsALDH and OsPBZ1 was examined in *Nicotiana benthamiana* leaves. OsALDH predominantly localized to the cytoplasm, whereas OsPBZ1 showed both cytoplasmic and nuclear localization (Supplementary Fig. 18).

To investigate potential protein-protein interactions, yeast two-hybrid (Y2H) assays were performed using OsALDH and OsPBZ1 against three OsPIMT isoforms: OsPIMT1, OsPIMT2, and ΔOsPIMT2 (OsPIMT2 lacking the 56-amino-acid N-terminal extension). ΔOsPIMT2 represents the major PIMT isoform present during the late seed maturation phase and has previously been associated with repair of isoAsp-mediated damage in seed proteins [21.] The results revealed that OsALDH interacted with OsPIMT1 and ΔOsPIMT2, but not with full-length OsPIMT2. In contrast, OsPBZ1 interacted with all three OsPIMT isoforms (Fig. 7a).

To further validate these interactions *in-planta*, bimolecular fluorescence complementation (BiFC) assays were performed in transiently transformed *N. benthamiana* leaves. YFP fluorescence was detected in both the cytoplasm and nucleus when OsALDH was co-expressed with OsPIMT1 or ΔOsPIMT2, whereas no fluorescence signal was observed with full-length OsPIMT2. Conversely, co-expression of OsPBZ1 with OsPIMT1, OsPIMT2, or ΔOsPIMT2 resulted in strong YFP fluorescence in both the cytoplasm and nucleus (Fig. 7b).

To confirm direct physical interactions, *in-vitro* pull-down assays were carried out using MBP-tagged OsALDH or OsPBZ1 together with GST-tagged OsPIMT1 recombinant proteins. These assays further confirmed direct interaction of OsPIMT1 with both OsALDH and OsPBZ1 (Fig. 7c).

To further substantiate these interactions *in-vivo*, co-immunoprecipitation assays were performed using YFP- and MYC-tagged fusion proteins transiently expressed in *N. benthamiana* leaves. PIMT1:YFP co-purified with either OsALDH:MYC or OsPBZ1:MYC following immunoprecipitation with anti-MYC antibodies when the respective fusion proteins were co-expressed (Fig. 7d). Notably, the bands observed around ~27 kDa likely correspond to the native PIMT protein of *N. benthamiana* that cross-reacted with the anti-PIMT antibody used for immunoblotting. Together with the Y2H, BiFC, and pull-down analyses, these findings firmly established OsALDH and OsPBZ1 as bona fide interactors and potential substrate proteins of PIMT.

Overexpression of *OsALDH* provides tolerance against *R. solani*

To further investigate the involvement of OsALDH and OsPBZ1 in sheath blight (ShB) defense, we analyzed their expression profiles following *R. solani* infection and jasmonic acid (JA) treatment. Both genes showed significant transcriptional induction under these conditions (Fig. 8a, b; Supplementary Fig. 19 a, b), supporting their potential roles in JA-mediated defense responses. While OsPBZ1 is well established as a broad-spectrum defense-related protein against bacterial and fungal pathogens[42,44], the contribution of OsALDH to biotic stress responses has remained largely unexplored.

To elucidate the functional role of OsALDH during ShB infection, we transiently overexpressed *OsALDH* in rice sheaths of WT and *pimt1* mutant plants. Successful overexpression was confirmed by transcript analysis (Fig. 8c). Upon *R. solani* infection, WT plants overexpressing OsALDH (*WT:OsALDH*) exhibited markedly reduced disease symptoms compared with vector control plants (*WT:VC*). In contrast, this protective effect was substantially compromised in the *pimt1* mutant background, as *pimt1:OsALDH* plants displayed more severe disease symptoms than *WT:OsALDH* plants (Fig. 8d). These observations were further supported by quantitative measurements of relative vertical sheath colonization (RVSC) and pathogen load, both of which were significantly lower in *WT:OsALDH* plants compared with *pimt1:OsALDH* plants (Fig. 8e, f). Together, these results demonstrate that OsALDH enhances ShB tolerance

Given our earlier findings that PIMT repairs stress-induced isoAsp accumulation in OsALDH *in-vitro*, we next examined isoAsp levels in Myc-tagged OsALDH expressed in WT and *pimt1* mutant backgrounds. Immunoprecipitation of OsALDH using anti-Myc antibodies from infected tissues revealed substantially lower isoAsp accumulation in OsALDH immunoprecipitated from WT compared with the *pimt1* mutant (Fig. 8g). These findings suggest that PIMT-mediated repair of isoAsp damage is required to maintain OsALDH functionality during pathogen infection.

To further validate the protective role of OsALDH, WGA-FITC staining and 3D imaging were performed to visualize fungal invasion within infected sheaths. *WT:OsALDH* plants exhibit a pronounced restriction

in fungal penetration depth and reduced formation of dense mycelial mats compared with *WT:VC* and *pimt1:OsALDH* plants (Fig. 8h, i), consistent with their enhanced disease tolerance.

As OsALDH is known to function in aldehyde detoxification and ROS scavenging[39,40], we next examined ROS accumulation and associated cellular damage. DAB staining revealed reduced ROS accumulation in *WT:OsALDH* plants relative to *WT:VC* and *pimt1:OsALDH* plants (Fig. 8j). Correspondingly, trypan blue staining showed significantly lower levels of host cell death in *WT:OsALDH* plants (Fig. 8k). Quantitative measurements further confirmed reduced H_2O_2 and MDA accumulation in *WT:OsALDH* plants, indicating reduced oxidative stress and membrane damage (Fig. 8l, m).

Because callose deposition is an important defense mechanism during rice *R. solani* interactions[4546], we also assessed callose accumulation in these plants. Aniline blue staining revealed enhanced callose deposition in *OsALDH*-overexpressing tissues, accompanied by elevated expression of the callose synthase gene *OsGSL5* (Supplementary Fig. 20). These observations suggest that OsALDH-mediated defense may additionally contribute to strengthening cell wall-associated immunity during pathogen infection.

Collectively, these findings support a model in which OsALDH enhances ShB tolerance by promoting ROS detoxification, reducing cellular damage, and strengthening host defense responses.

OsALDH and OsPBZ1 inhibit fungal growth

To further elucidate the direct antifungal roles of OsALDH and OsPBZ1 against *R. solani*, and to determine how isoAsp accumulation influences their enzymatic functions *in-vivo*, we performed antifungal assays using *R. solani* sclerotia, as described previously[47]. Individual sclerotia were treated with equal concentrations of bacterially purified OsALDH or OsPBZ1 (Control), H_2O_2-treated OsALDH or OsPBZ1 to induce isoAsp formation (Treated), or H_2O_2-treated proteins subsequently incubated with OsPIMT1 and AdoMet to facilitate repair (Repaired). Additional controls included treatments with purified OsPIMT1 alone or buffer alone. Following treatment, the sclerotia were allowed to germinate on PDA plates and were evaluated for radial hyphal growth.

Treatment with control OsALDH or OsPBZ1 markedly inhibited fungal proliferation, an effect that was clearly visible as early as 2 dpi (Fig. 9a). In contrast, H_2O_2-treated OsALDH or OsPBZ1, which accumulated isoAsp modifications, exhibited substantially reduced antifungal activity, resulting in enhanced fungal growth comparable to buffer-treated controls. Notably, incubation of the oxidatively damaged proteins with active OsPIMT1 in the presence of AdoMet restored their antifungal capacity, leading to strong suppression of fungal growth similar to that observed with untreated proteins. Quantification of radial fungal growth further confirmed that both OsALDH and OsPBZ1 significantly restricted the growth of *R. solani*, whereas oxidative damage impaired this activity and PIMT-mediated repair play a significant role in it (Fig. 9b, c). Importantly, treatment with OsPIMT1 alone had no direct effect on fungal growth, indicating that PIMT itself does not possess any antifungal activity (Supplementary Fig. 21).

Collectively, these findings demonstrate that OsALDH and OsPBZ1 possess strong antifungal activities against *R. solani*

Previous studies have shown that pathogen-induced ROS play critical roles in fungal biology[48]. In particular, necrotrophic fungi actively regulate ROS production to support their development and enhance virulence[49,50]. ROS accumulation within fungal hyphae has also been linked to the transcriptional regulation of antioxidant genes, which collectively help fungi alleviate oxidative stress and promote host tissue necrosis[51]. Given the established antioxidant functions of OsALDH, we hypothesized that its antifungal activity against *R. solani* may be associated with disruption of fungal ROS homeostasis.

To test this hypothesis, intracellular ROS accumulation in fungal hyphae was assessed using H_2DCFDA staining and subsequent quantification. Significantly reduced ROS accumulation was observed in hyphae treated with active OsALDH compared with buffer-treated controls, H_2O_2-treated samples (positive control), or oxidatively damaged/inactivated OsALDH proteins (Fig. 9d, e). Importantly, hyphae treated with PIMT-repaired OsALDH also showed minimal fluorescence, similar to those treated with native active

OsALDH. These observations suggest that functional OsALDH disrupts the ROS balance required for normal fungal growth and development, thereby suppressing fungal proliferation as observed in Fig. 9a.

To further examine the impact of OsALDH on fungal development, the ultrastructure of *R. solani* hyphae was analyzed using scanning electron microscopy (SEM). Hyphae exposed to OsALDH displayed severe morphological abnormalities, appearing wrinkled, collapsed, and exhibiting reduced hyphal branching compared with the smooth and intact mycelial structures observed in untreated controls (Fig. 9f). These structural defects further support the inhibitory effects of OsALDH on fungal growth and development. However, a more detailed mechanistic understanding will be required to fully exploit the antifungal potential of OsALDH.

Collectively, our findings demonstrate that *OsPIMT*s enhance sheath blight tolerance in rice by interacting and maintaining the function of stress-damaged OsALDH and OsPBZ1 proteins. In turn, OsALDH and OsPBZ1 exhibit potent antifungal activities against *R. solani*, thereby contributing to enhanced disease resistance (Fig. 10).

Discussion

Rice ShB, caused by *R. solani*, remains one of the most destructive diseases limiting global rice production. To survive pathogen attack, rice plants deploy multilayered defense mechanisms involving rapid stress perception and activation of molecular, biochemical, and physiological responses. Proteins play central roles in these processes; however, they are highly vulnerable to oxidative damage caused by excessive reactive oxygen species (ROS) accumulation during stress. Oxidative stress not only disrupts protein structure and function but also promotes the formation of abnormal residues such as isoaspartate (isoAsp), which can impair protein stability and enzymatic activity. To counteract such damage, plants have evolved protein repair systems, among which PIMT, represents a crucial component that repairs isoAsp-containing proteins. Although PIMT has been extensively associated with seed longevity, abiotic stress tolerance, and maintenance of ROS homeostasis through repair of antioxidant enzymes such as APX, CAT, and SOD, its contribution to biotic stress responses has remained largely unexplored. In this study, we demonstrate that

PIMT plays a central role in maintaining protein integrity and promoting rice tolerance against *R. solani* infection.

ROS accumulation is one of the earliest hallmarks of the rice- *R. solani* interaction and functions as an important defense signal[36,52]. However, necrotrophic pathogens such as *R. solani* exploit excessive ROS accumulation to accelerate host cell death and facilitate nutrient acquisition [11]. Therefore, the outcome of infection largely depends on the host's ability to maintain ROS homeostasis. Antioxidant enzymes including APX, CAT, and SOD constitute the primary defense system that detoxifies excess ROS and limits oxidative damage. Previous studies have shown that overexpression of antioxidant proteins enhances tolerance to *R. solani* by alleviating oxidative injury[53]. Nevertheless, how plants preserve the functional integrity of these enzymes under prolonged pathogen-induced oxidative stress has remained unclear. Our findings address this gap by uncovering a protein repair-based defense mechanism that sustains antioxidant function during fungal infection.

We observed that both ROS accumulation and isoAsp levels progressively increased during *R. solani* infection, suggesting a association between oxidative stress and protein damage during disease progression (Fig.1). Functional analyses using overexpression, RNAi, and CRISPR/Cas9-mediated mutant lines provided strong genetic evidence for the protective role of PIMT (Fig. 2, 4). *OsPIMT* overexpression enhanced ShB tolerance by restricting fungal colonization, penetration, and disease progression, whereas *pimt1* mutant lines exhibited severe disease symptoms, elevated ROS accumulation, increased membrane damage, and enhanced pathogen proliferation. Consistently, H_2DCFDA and DAB staining demonstrated reduced ROS accumulation in overexpression lines, while lower MDA levels indicated diminished lipid peroxidation and improved membrane integrity (Fig. 3, 5). In contrast, *pimt* mutants displayed compromised growth and reduced yield-associated traits, emphasizing the broader importance of PIMT in maintaining cellular homeostasis (Supplementary Fig. 7). Together, these findings establish a previously unrecognized role of PIMT as an additional protective layer during biotic stress, extending its known functions beyond seed vigor, longevity, and abiotic stress tolerance[21,22,25,28,29].

Plant immunity against microbial pathogens is largely coordinated through salicylic acid (SA)- and jasmonic acid (JA)-mediated signaling pathways. While SA signaling predominantly mediates resistance against biotrophic pathogens, JA signaling is critical for defense against necrotrophs such as *R. solani*[54–56]. Our results establish a strong association between PIMT activity, JA accumulation, and disease tolerance. PIMT-overexpressing plants displayed enhanced resistance, whereas *pimt* mutants exhibited pronounced susceptibility accompanied by reduced JA accumulation and downregulation of defense-related genes (Supplementary Fig. 1, 4, 12). These observations suggest that PIMT-mediated protein repair not only preserves antioxidant capacity but may also contribute to maintaining JA-dependent defense signaling during infection.

To elucidate the mechanistic basis of PIMT-mediated tolerance, we identified potential PIMT-interacting proteins through IP-MS/MS analysis (Supplementary Table S1). Along with known antioxidant enzymes, two defense-associated proteins OsALDH and OsPBZ1 were identified as prominent PIMT interactors. Both *R. solani* infection and H_2O_2 treatment induced isoAsp formation in OsALDH and OsPBZ1, whereas catalytically active OsPIMT1 efficiently reduced isoAsp accumulation and restored protein function (Fig. 6). In contrast, catalytically inactive PIMT variants failed to repair the damaged proteins. Importantly, oxidative stress-induced isoAsp accumulation substantially impaired the enzymatic activities of both proteins, and this functional loss was reversed in the presence of OsPIMT1. These findings suggest a direct mechanistic link between oxidative protein damage and PIMT-mediated restoration of defense-associated protein activity.

Although OsPIMT1 emerged as a major repair enzyme, as compared to OsPIMT2 in our analyses, the involvement of additional isoforms cannot be excluded. Protein-protein interaction assays revealed that OsALDH and OsPBZ1 interact with OsPIMT2 and/or ΔOsPIMT2, suggesting the existence of potentially isoform-specific and tissue-specific repair mechanisms (Fig. 6). Such diversification may provide plants with an adaptive advantage by enabling precise regulation of protein repair under distinct developmental stages or stress conditions.

Both OsALDH and OsPBZ1 were strongly induced during *R. solani* infection and JA treatment, supporting their involvement in JA-mediated defense responses. OsPBZ1 is a well-characterized intracellular ribonuclease implicated in resistance against rice blast disease[41,57]. In contrast, the role of OsALDH in biotic stress responses had remained largely unexplored. Aldehyde dehydrogenases constitute a diverse protein family involved in seed maturation, ROS homeostasis, and abiotic stress tolerance[39,58,59], although only a few family members have been linked to disease resistance. For example, OsALDH2b contributes to resistance against bacterial and fungal pathogens through a moonlighting transcriptional regulatory function rather than its enzymatic activity[60]. OsALDH7 has also been associated with aldehyde detoxification and maintenance of seed viability[40,61]. Our study now identifies a distinct role for OsALDH in ShB tolerance. Potential functional relevance of PIMT and its interacting partners in mitigating *X. oryzae* or *M. oryzae* infection remains an open question, not addressed yet experimentally.

Transient overexpression of OsALDH in WT plants significantly reduced disease severity, fungal colonization, and pathogen load following *R. solani* infection. Microscopic analyses further demonstrated restricted fungal penetration and reduced mycelial proliferation in OsALDH-overexpressing tissues. Mechanistically, these observations are consistent with the established ROS-scavenging and aldehyde-detoxifying functions of ALDH proteins (Fig. 8)[59,61]. *WT:OsALDH* plants displayed reduced ROS accumulation, lower H_2O_2 and MDA levels, and diminished host cell death, collectively indicating enhanced oxidative stress management. Importantly, these protective effects were severely compromised in the *pimt1* mutant plants (Fig. 8).

Our *in-vitro* antifungal assays further revealed that both OsALDH and OsPBZ1 possess direct antifungal activity against *R. solani*. Treatment of fungal sclerotia with functional proteins strongly inhibited fungal growth, whereas oxidatively damaged proteins lost much of this activity. Notably, the antifungal activity of OsALDH appears to be associated with disruption of fungal ROS homeostasis (Fig. 9). Since ROS are required for normal fungal growth and pathogenicity in necrotrophic fungi[51-54], interference with fungal ROS regulation may represent an effective defense strategy. Consistent with this hypothesis, OsALDH

treatment reduced intracellular ROS accumulation within fungal hyphae and induced severe ultrastructural abnormalities, including collapsed and distorted hyphal morphology. However, the precise molecular mechanisms underlying the antifungal activities of OsALDH and OsPBZ1 remain to be elucidated.

Collectively, our findings establish PIMT as a critical protein repair factor that preserves the functionality of multiple defense-associated proteins during pathogen infection. By repairing isoAsp-mediated protein damage, PIMT counteracts the pathogen-induced collapse of antioxidant and defense systems, thereby sustaining host cellular homeostasis during necrotrophic stress. The identification of additional putative PIMT substrates, including antioxidant enzymes, sucrose transporters, and lignin biosynthesis-related proteins, further suggests the existence of a broad multilayered protein repair network operating during pathogen challenge (Supplementary Table 1).

In conclusion, this study uncovers involvement of PIMT in rice immunity and establishes a protein repair-based defense mechanism that enhances resilience against sheath blight disease. Our findings reveal that maintenance of protein functionality through isoAsp repair represents a crucial adaptive strategy during necrotrophic infection, thereby opening avenues for engineering durable disease resistance in crops (Fig. 10).

Methods

Plant Materials and growth condition

Rice cultivars *O. sativa L.* japonica (Taipei 309) and *O. sativa L.* indica (Pusa basmati-1) were used for this study. The rice cultivar PB1 and TP309 along with transgenic lines were grown in plant growth facility at 28ºC temperature, 80% relative humidity, and 16/8hr of day/night with 250µmol light intensity. We analyzed *OsPIMT1 (Os08g44280)* and *OsPIMT2 (Os04g40540)* constitutive overexpression (OE) lines, as well as intron-spliced hairpin RNA interference (RNAi) lines in *O. sativa L.* indica (Pusa basmati-1) background generated in our previous study[21,22]. *N. benthamiana* were grown in 3:1 combination of

agropeat and vermiculite, under growth room under long day conditions (16/8hr light and dark cycle at 22±2ºC, the light intensity of 100µmol m^{-2} s^{-1}) for general growth and seed harvesting.

Construct preparation

Two guide RNAs having minimum off-targets and maximum on-target scores were selected using CRISPR-P 2.0 tool (http://crispr.hzau.edu.cn/CRISPR2/), for Cas-9 mediated genome editing of *OsPIMT1* and *OsPIMT2*. The guide RNA, along with polycistronic transfer RNA and scaffold (sgRNA), was cloned into pRGEB32 vector using NEBridge® Golden Gate Assembly Kit (BsaI-HF® v2),[27,62]. For the transient overexpression of *OsALDH*, the CDS was amplified and cloned into the binary vector pCAMBIA1301 under the control of the *35s* promoter for constitutive expression [27]. OsALDH and OsPBZ1 coding sequences were cloned in a *pENTR-D-TOPO* (Invitrogen) vector and then subcloned into *pDEST566* vector to produce MBP tagged OsALDH and OsPBZ1 recombinant proteins using gateway technology. OsALDH and OsPBZ1 were subcloned in Yeast two-hybrid (Y2H) destination vectors pDEST-GADT7 (activation domain, AD) and pDEST-GBKT7 (binding domain, BD). OsALDH and OsPBZ1 were subcloned into pSITE BiFC-cEYFP-N1 vectors via pENTR/D-TOPO (Invitrogen) alongside our existing OsPIMTs vectors in pSITE BiFC nEYFP-C1 vector [22].

Generation of transgenic plants/transient expression in rice

The construct was mobilized in *Agrobacterium tumefaciens* LBA4404 and used for the agrobacterium mediated rice transformation. Rice (TP-309) seeds were surface-sterilized, and embryogenic calli were induced on callus induction medium containing 2mg/L 2,4-D. Five-day-old embryogenic calli were infected with *A. tumefaciens* strain LBA4404 harbouring the construct, followed by co-cultivation for 48hr. After washing with cefotaxime, calli were selected on medium supplemented with 50mg/L hygromycin and 500mg/L cefotaxime. Resistant calli were regenerated on media containing 2mg/L kinetin and 0.2mg/L NAA, and regenerated shoots were transferred sequentially to shooting and rooting media. Fully developed plantlets were maintained in Yoshida nutrient solution [22,27].

For the transient overexpression of *OsALDH*, agrobacterium cells carrying *CaMV35s: OsALDH* construct were injected into the sheaths of 45-day old WT or *pimt1* mutant rice plants using a syringe. Infiltered sheaths were inoculated with *R. solani* sclerotia 24hr after agrobacterium infiltration and sheathes were evaluated for the disease symptoms [11].

Sheath blight disease tolerance assay

The rice seedlings of wildtype and transgenic lines were grown in plant growth facility. Around 45 days old tillers of rice were inoculated with freshly prepared equal sized sclerotium of *R. solani* AG1-IA isolate BRS-1 [63]. The inoculation was performed on the second topmost collar of the tiller, just below leaf collar on the inner side of sheath as described in [64]. The plants were incubated in growth chamber and routinely manual water spraying was also carried out to keep high humidity that is conducive for ShB disease. The phenotypic observations were recorded at 1-, 2-, 3-, and 4-days post pathogen inoculation. The length of lesions was measured using ImageJ software. Lesion length data represents the average length of lesions from 10 lesions measured on multiple sheaths. The relative vertical sheath colonization (RVSC) was calculated by formula VSC/sheath length × 100[64]. At least, 10 tillers of each line were analysed in each experiment and experiments were independently repeated three times. The infected tillers were photographed using a DSLR camera. In each experiment uninfected tillers were used as a negative control. The diseased zone from each sample was harvested in liquid N_2 and were stored at -80ºC till further use for biochemical analysis.

Protein extraction, PIMT Activity and isoAsp quantification assay

Total crude proteins were extracted in protein extraction buffer containing 100mM HEPES buffer, pH7.5, 2mM β-mercaptoethanol, 10% glycerol, 10mM Sodium metabisulphite and Protease inhibitor cocktail. The suspensions were centrifuged at 15493x g for 15min at 4°C. The supernatants were collected and stored at -80°C. Extracted protein was used for different biochemical analysis[21].. Protein concentration was estimated using bradford assay[65]. PIMT-specific activity was calculated by subtracting isoAsp peptide-independent

(endogenous) activity from isoAsp peptide-dependent activity. ISOQUANT isoAsp detection kit (Promega, Madison, WI, USA) was used for the estimation of isoAsp according to the kit's protocol [66].

Quantitative real-time PCR

Total RNA was extracted and RT-qPCR was carried as described in[67] on an ABI step one real time PCR using suitable primers (Supplementary Table 3). The expression of genes was normalized to the expression of *OsUBQ10/Os17s rRNA*. For the fungal biomass in the infected samples was quantified using the $2^{-\Delta Ct}$ method, wherein ΔCt is the difference between the cycle threshold (Ct) values of the fungal *Rs18s rRNA* (target) and host *OsUBQ10/Os17s rRNA*[36,68].

WGA-FITC and H_2DCFDA staining

Infected sheath tissue samples were cut into 2cm pieces and autoclaved in 1M KOH (HiMedia). After removing KOH from the autoclaved samples, 50mM Tris pH 7.0 was added, and samples were incubated at room temperature for 15-20 min. Tissue was transferred into MCTs having 20µg/µL WGA-FITC stain (Sigma), incubated for 30min at room temperature. After staining, tissue was gently washed with 50mM TrisCl pH 7.0, followed by wash with water[68]. Sample were then observed under GFP filter in TCS-SP8 Leica laser confocal microscope. Images were analyzed using LAS AF build 7266 software, and a topological 3D image was created to quantify the depth of pathogen penetration.

For cellular ROS localization, sheath tissue was cut into a transverse section and put in 5µM H_2DCFDA stain (prepared in DMSO) for 10min and observed under GFP filter in confocal laser scanning microscope (Leica TCS-SP8).

To observe callose, transverse sections of sheaths were stained for 10min at room temperature with 0.01% (w/v) aniline blue in 0.1M phosphate buffer (pH 8.5). After being washed with phosphate buffer, sections were visualized under DAPI filter with a confocal laser scanning microscope (Leica TCS-SP8). The experiments were performed with three independent biological replicates.

Immunoprecipitation

Total proteins were extracted from infected rice sheath tissue in IP lysis buffer 50mM TrisCl, 150mM NaCl, 1% Triton, 1mM EDTA, 1mM MgCl2, and a protease inhibitor cocktail. The resulting protein extract then underwent immunoprecipitation with an anti-PIMT antibody[27,69]. Immunoprecipitation was subsequently conducted for 2-3 hr at 4°C with gentle shaking, employing Protein G Dynabeads to capture the complexes. The Dynabeads were then rinsed three times using the washing buffer provided with the Dynabeads Protein G immunoprecipitation kit (Thermo Scientific). Bound proteins were eluted directly into SDS loading dye, which facilitated their subsequent separation on a 12% SDS-PAGE.

Sample preparation and LC-MS/MS analysis

Protein bands were carefully excised from the gel. These excised gel pieces then underwent in-gel tryptic digestion[28]. After tryptic digestion, the resultant peptides were vacuum-dried and then reconstituted in 0.1% formic acid, preparing them for downstream LC-MS/MS analysis. This analysis was performed on an AB Sciex 400 Triple TOF 6600 mass spectrometer, integrated with an Ekspert nano-LC 425[27].

Samples were concentrated using an Eksigent Nano Trap Cartridge (Chrome XP; C18-CL, 3 μm, 120 Å pore size; 350 μm × 0.5 mm), and the concentrated peptides were separated using an Eksigent capillary reverse-phase column (Chrome XP, 3C18-CL-120, 3 μm, 120 Å, 0.075 × 150 mm). Separation was performed at a flow rate of 300 nL/min using solvent A (2% acetonitrile with 0.1% formic acid [vol/vol] in MS-grade water) and solvent B (98% acetonitrile with 0.1% formic acid [vol/vol]). The gradient program was 2 to 50% solvent B over 60 min, followed by 50 to 90% solvent B over 1 min, 90% solvent B for 3 min, and 90 to 5% solvent B over 0.5 min, with a final re-equilibration at 2% solvent B for 2.5 min. Mass spectra and tandem mass spectra were recorded in positive-ion, high-sensitivity mode with a full-scan resolution of 35,000. Ion source parameters were as follows: ion spray voltage floating (ISVF) = 2,400, ion source gas 1 (GS1) = 13, ion source gas 2 (GS2) = 0, and curtain gas flow (CUR) = 10. Precursor ions were fragmented using nitrogen gas in a collision cell. TOF-MS and TOF-MS/MS spectra were calibrated with 100 fmol beta-galactosidase digest (SCIEX), and peptide and MS/MS spectra were recorded over m/z ranges of 350 to 1,500 and 200 to 1,600, respectively, in data-dependent acquisition (DDA) mode.

Raw LC-MS/MS data were initially processed using Analyst 1.7 (AB Sciex). Subsequent peptide and protein identification was performed using the Paragon method implemented in Protein Pilot v5.0.1, following the guidelines described in[22]. Peak lists generated were searched against the UniProt *Oryza sativa* proteome database, encompassing 453,874 protein entries. The database interrogation in Protein Pilot employed standard tryptic peptides, permitting up to three missed cleavages. Identifications were validated with a 1% false discovery rate (FDR). Mass tolerances were configured at 0.7Da for-precursor ions and 0.6Da for-fragment ions, respectively. Individual spectra were deemed acceptable for identification based on a confidence threshold of 95% and an unused score exceeding 1.3.

Immunoblotting, Co-IP and Pull-down assay

For immunoblotting of PIMT proteins from plant extracts equal concentrations were separated via 12% SDS-PAGE, and separated proteins were electroblotted onto a polyvinylidene difluoride (PVDF) membrane. PIMT proteins were identified using OsPIMT primary antibodies [21] (1:5000), For loading control, tubulin was detected with an anti-tubulin antibody (Sigma Aldrich T9028- 1:10000). Western blot quantification was done by ImageJ software by normalizing PIMT protein band intensity to tubulin control band intensity.

GST alone and recombinant GST-OsPIMT1 were used as baits on glutathione superflow resin before incubating them with the recombinant MBP-OsALDH and MBP-OsPBZ1 protein. After washing with 1X PBS, the complex was eluted using 10mM reduced glutathione. The eluted complex was used for immunoblotting using an MBP antibody (Agrisera Cat No AS153309, 1:10000) and an anti-GST antibody (Sigma Cat No G7781-100µL, 1:5000).

For co-immunoprecipitation assays, the PIMT1 and ALDH or PBZ1 proteins were transiently co-expressed in *N. benthamiana* leaves. Total proteins were extracted following the protocol described above, and immunoprecipitated with anti-MYC antibodies employing Protein G Dynabeads to capture the complexes following the outlined procedure in earlier section. The eluates were separated by SDS-PAGE and analyzed

by immunoblotting using anti-PIMT (1:5000) and anti-MYC (Sigma, C3966-1:5000) primary antibodies. Immunoreactive proteins were detected by chemiluminescence using an anti-rabbit secondary antibody[21].

Protein damage and PIMT repair assay

To investigate oxidative stress effects, purified 50µg recombinant OsALDH, OsPBZ1 proteins were incubation with 30mM H_2O_2 at 25°C for 4hr[28,70]. Treated samples were analyzed for isoAsp accumulation using the ISOQUANT isoAsp detection kit (Promega), following the outlined procedure in earlier section[28]. For LC-MS/MS analysis samples were subjected to 12% SDS-PAGE. Subsequently, in-gel trypsin digestion was carried out, followed by LC–MS/MS analysis to identify protein modifications as described earlier. ESI mass spectra of tryptic peptides were acquired using protein pilot software [28]. To assess PIMT repair capabilities, H_2O_2 -treated OsALDH, OsPBZ1, served as a substrate, in reactions with enzymatically active (OsPIMT1) and inactive (OcPIMT1-2) PIMT [22]. These repair reactions were conducted for 1hr at 37°C, comprising 30µM PIMT and 10µM AdoMet in 0.1M HEPES buffer (pH 7.5).

Post-repair, isoAsp content was re-evaluated using ISOQUANT isoAsp detection kit (Promega), following the outlined procedure in earlier section[28].

Anti- fungal plate assay and Reactive oxygen species imaging in *R. solani*

Individual *R. solani* sclerotia were treated for 12hr at 28°C with 20µg/ml of bacterially purified OsALDH or OsPBZ1 (Control); purified OsALDH or OsPBZ1 treated with H_2O_2 to induce isoAsp formation (Treated); and H_2O_2-treated OsALDH or OsPBZ1 subsequently repaired with PIMT1 (Repaired). The treated sclerotia were placed onto freshly prepared PDA plates, and upon incubation at 28°C, sclerotia germination and fungal growth as the diameter (in cm) of the mycelial lawn at different time points (2- and 4-days dpi) was recorded. Growing mycelia were placed on sterile glass slides, stained with 10µM H_2DCFDA (Thermo Fisher Scientific Inc.) and visualized under GFP filter of Confocal Laser Scanning Microscope (TCS-SP5, Leica, Germany). The images were analysed using LAS AF build 7266 software. Experiments were repeated using three biological replicates. For scanning electron microscopy analysis of *R. solani* mycelia; mycelia placed on the surface of a microscopic slide in a low-vacuum scanning electron

microscope. SEM images were captured on a ZEISS EVO LS 10 with an electron high distance of 20.00kV at magnifications of 500x and 2000x.

RNAse Activity Assay

RNAse activity assay was performed with control, treated and repaired OsPBZ1 protein using Abcam RNAse activity assay kit (ab273299) according to manufacturer's protocol.

ALDH activity Assay

Aldehyde dehydrogenase activity assay was performed according to[43] protocol with minor modifications. Reaction mixture contained 100mM PBS, 1.3mM NAD+ and 100µM acetaldehyde and a volume of protein extracts from transformed *E. coli BL21DE3* cells in a total volume of 100µl. The reaction was initiated by addition of acetaldehyde. ALDH activity was evaluated from the rate of increase in absorbance at 340nm due to the conversion of NAD+ to NADH.

Histochemical staining

3,3′-diaminobenzidine (DAB) histochemical staining was used to detect H_2O_2 accumulation in rice [35,71]. Rice sheath samples were incubated in 1mg mL^{-1} DAB prepared in 50mM Tris-acetate buffer (pH 5.0) at 25°C in the dark for 16hr, followed by destaining in ethanol:glycerol:acetic acid (3:1:1). H_2O_2 accumulation was visualized as brown precipitates.

Host cell death was assessed by staining infected sheaths with 0.02% trypan blue overnight, followed by destaining and imaging [35]. Images were acquired using a Nikon camera.

Quantification of H_2O_2 and MDA

MDA was quantified using 50mg of sheath tissue homogenized with 2mL of 0.25% (w/v) thiobarbituric acid prepared in 10% (w/v) TCA. Homogenate was incubated at 95°C for 30min and then was kept in an ice bath for 10 min. Homogenate was then centrifuged at 15493 x g for 30min. The absorbance of the supernatant was measured at 532nm and 600nm [70,72]. The nonspecific absorbance of the supernatant at 600nm was deducted from the absorbance of 532nm, and the difference was used to determine the concentration of MDA using the extinction coefficient of 155mM^{-1} cm^{-1}. H_2O_2 was quantified following

the method[73,74] using 100mg of sheath tissue homogenized in 2mL of 0.1% TCA. Homogenate was centrifuged at 15493 x g for 20min at 4°C. The supernatant was mixed with an equal volume of 10mM potassium phosphate buffer (pH 7.0) and a double volume of 1M potassium iodide and kept in the dark for 1h at room temperature. The absorption of the supernatant was measured at 390nm. The amount of H_2O_2 was calculated using a standard curve prepared from known concentrations of H_2O_2.

Catalase (CAT) and ascorbate peroxidase (APX) activity

Catalase activity was determined as described in[75]. Fifty millimolar potassium phosphate buffer (pH 7.8), 3mM H_2O_2 and 20µl total protein extract was added to 200µl reaction. At 240nm, the decomposition of H_2O_2 by CAT was monitored. Ascorbate peroxidase activity was measured as described in[28,76]. Total reaction mix contained 50mM potassium phosphate buffer (pH 7.8), 0.5mM ascorbic acid (ASA) and 0.5mM H_2O_2 with 20µl of protein extract in 200µl reaction. Ascorbate peroxidase activity was determined by measuring the decrease in the absorbance of ASA at 290nm at 25°C caused by oxidation by H_2O_2. The activity of APX was calculated using an extinction coefficient of 2.8mM^{-1} cm^{-1}.

Bacterial over expression and purification of recombinant protein

Recombinant proteins were expressed in *E.coli BL21DE3* cells at 18ºC. The bacterial cells were collected by centrifugation at 15493 x g at 4ºC and lysed by sonication in a buffer containing 20mM TrisCl pH 7.6, 150mM NaCl, and 10mM β-mercaptoethanol with bacterial protease inhibitor cocktail (Sigma) and 2mM PMSF (Sigma). The extracts were analysed by 12% SDS PAGE and purified using affinity column chromatography[22]. For purification of MBP tagged OsALDH and OsPBZ1, dextrin amylose MBP resin (G-Biosciences) was used.

Defense hormone estimation

For phytohormones estimation frozen samples were ground into a fine powder using a tissue lyser. Samples were dissolved in ice-cold methanol containing labeled internal standards. Dissolved samples were mixed on a rotator shaker followed by centrifugation at 15493 x g for 30mins. Samples were vacuum-dried and

dissolved in ice-cold methanol. A triple-quadruple LC-MS/MS system (QTRAP 6500^{+}) was used for phytohormone quantification[77].

Bimolecular Fluorescence Complementation (BiFc)

pSITE BiFC-cEYFP-N1 and pSITE BiFC nEYFP-C1 vectors were transformed into Agrobacterium and co-infiltrated in *N. benthamiana* leaves in different combination [22] and imaged to study the protein-protein interactions.

Y2H analysis

To investigate protein-protein interactions between OsALDH and OsPBZ1 our existing BD-OsPIMT vectors were co-transformed with AD:OsALDH or AD:OsPBZ1 into the Y2H Gold yeast strain (Clonetech) using the EZ-Yeast Transformation Kit (MP Biomedicals) as per the manufacturer's protocol [78,79].

Statistical Analysis

Statistical tests were performed in SPSS23 software and GraphPad Prism 8.0. Error bars indicate mean ± SE. Different letters in the Figures indicate the analysis of variance (ANOVA) using Tukey's post hoc test ($P < 0.05$) (for exact P-values, see Source Data). P values were determined by unpaired t-test using GraphPad Prism 8.0 (for exact P-values, see Source Data).

Data availability

The proteomics data generated in this study have been deposited to the ProteomeXchange Consortium via the PRIDE partner repository with the dataset identifier PXD080366. The sequence of the major genes in this study is available at Rice Genome Annotation Project (https://rice.uga.edu/) under the accession numbers: *OsPIMT1, LOC_Os08g44280; OsPIMT2, LOC_Os04g40540; OsALDH7, LOC_Os09g26880; OsPBZ1, LOC_Os12g36880; OsPR5, LOC_Os12g43430; OsAOS1, LOC_ Os03g55800; OsAOC, LOC_Os03g32314; OsGSL5, LOC_Os06g08380; OsLOX, LOC_Os08g39840* and in *R. solani* genome database *Rs17srRNA, MK481078.1*. The original data presented in the study are included in the article/Supplementary Figures, Tables and Data; further inquiries can be directed to the corresponding author. Source data are provided with this paper.

References

1. Molla, K. A. *et al.* Understanding sheath blight resistance in rice: the road behind and the road ahead. *Plant Biotechnol. J.* **18**, 895–915 (2020).

2. Zheng, A. *et al.* The evolution and pathogenic mechanisms of the rice sheath blight pathogen. *Nat. Commun. 2013 41* **4**, 1–10 (2013).

3. Choudhury, F. K., Rivero, R. M., Blumwald, E. & Mittler, R. Reactive oxygen species, abiotic stress and stress combination. *Plant J.* **90**, 856–867 (2017).

4. Qi, J., Wang, J., Gong, Z. & Zhou, J. M. Apoplastic ROS signaling in plant immunity. *Curr. Opin. Plant Biol.* **38**, 92–100 (2017).

5. Mittler, R., Zandalinas, S. I., Fichman, Y. & Van Breusegem, F. Reactive oxygen species signalling in plant stress responses. *Nat. Rev. Mol. Cell Biol. 2022 2310* **23**, 663–679 (2022).

6. Liu, H. *et al.* The Class III peroxidase gene OsPrx30, transcriptionally modulated by the AT-hook protein OsATH1, mediates rice bacterial blight-induced ROS accumulation. *J. Integr. Plant Biol.* **63**, 393–408 (2021).

7. Wally, O., Jayaraj, J. & Punja, Z. Comparative resistance to foliar fungal pathogens in transgenic carrot plants expressing genes encoding for chitinase, β-1,3-glucanase and peroxidise. *Eur. J. Plant Pathol. 2008 1233* **123**, 331–342 (2008).

8. Wally, O. & Punja, Z. K. Enhanced disease resistance in transgenic carrot (Daucus carota L.) plants over-expressing a rice cationic peroxidase. *Planta 2010 2325* **232**, 1229–1239 (2010).

9. Wang, A. *et al.* Identification of rice (Oryza sativa L.) genes involved in sheath blight resistance via a genome-wide association study. *Plant Biotechnol. J.* **19**, 1553–1566 (2021).

10. Xie, W. *et al.* Knockout of transcription factor OsERF65 enhances ROS scavenging ability and confers resistance to rice sheath blight. *Mol. Plant Pathol.* **24**, 1535–1551 (2023).

11. Sahoo, D., Chandan, R. K., Goel, N. & Jha, G. OsNUOR enhances disease susceptibility by interfering with reactive oxygen species homeostasis and ferroptosis-like cell death. *Plant Cell* (2026) doi:10.1093/PLCELL/KOAG112.

12. Tripathy, B. C. & Oelmüller, R. Reactive oxygen species generation and signaling in plants. *Plant Signal. Behav.* **7**, 1621–1633 (2012).

13. Clarke, S. Aging as war between chemical and biochemical processes: Protein methylation and the recognition of age-damaged proteins for repair. *Ageing Res. Rev.* **2**, 263–285 (2003).

14. Kamble, N. U. & Majee, M. Protein l-isoaspartyl methyltransferase (PIMT) in plants: Regulations and functions. *Biochem. J.* **477**, 4453–4471 (2020).

15. Mudgett, M. B. & Clarke, S. Characterization of plant L-isoaspartyl methyltransferases that may be involved in seed survival: Purification, cloning, and sequence analysis of the wheat germ enzyme. *Biochemistry* **32**, 11100–11111 (2002).

16. Mcfadden, P. N. & Clarket, S. Conversion of isoaspartyl peptides to normal peptides: Implications for the cellular repair of damaged proteins (protein methylation/carboxyl methyltransferase/erythrocyte). *Biochemistry* **84**, 2595–2599 (1987).

17. Ogé, L. *et al.* Protein Repair l-Isoaspartyl Methyltransferase1 Is Involved in Both Seed Longevity and Germination Vigor in Arabidopsis. *Plant Cell* **20**, 3022–3037 (2008).

18. Nayak, N. R. *et al.* An Arabidopsis ATP-Dependent, DEAD-Box RNA Helicase Loses Activity upon IsoAsp Formation but Is Restored by PROTEIN ISOASPARTYL METHYLTRANSFERASE. *Plant Cell* **25**, 2573–2586 (2013).

19. Verma, P. *et al.* PROTEIN l-ISOASPARTYL METHYLTRANSFERASE2 Is Differentially Expressed in Chickpea and Enhances Seed Vigor and Longevity by Reducing Abnormal Isoaspartyl Accumulation Predominantly in Seed Nuclear Proteins. *Plant Physiol.* **161**, 1141–1157 (2013).

20. Wei, Y. *et al.* Protein repair l -isoaspartyl methyltransferase 1 (PIMT1) in rice improves seed longevity by preserving embryo vigor and viability. *Plant Mol. Biol. 2015 894* **89**, 475–492 (2015).

21. Petla, B. P. *et al.* Rice PROTEIN l-ISOASPARTYL METHYLTRANSFERASE isoforms differentially accumulate during seed maturation to restrict deleterious isoAsp and reactive oxygen species accumulation and are implicated in seed vigor and longevity. *New Phytol.* **211**, 627–645 (2016).

22. Kamble, N. U. & Majee, M. ABI transcription factors and PROTEIN L-ISOASPARTYL METHYLTRANSFERASE module mediate seed desiccation tolerance and longevity in Oryza sativa. *Dev.* **149**, (2022).

23. Zhang, Y. *et al.* Maize PIMT2 repairs damaged 3-METHYLCROTONYL COA CARBOXYLASE in mitochondria, affecting seed vigor. *Plant J.* **115**, 220–235 (2023).

24. Zhang, Y. *et al.* Natural variation in the ZmPIMT1 promoter enhances seed aging tolerance by regulating PABP2 repair in maize. *Plant Cell* **37**, 217 (2025).

25. Kamble, N. U. *et al.* PROTEIN L-ISOASPARTYL METHYLTRANSFERASE protects enolase dysfunction by repairing isoaspartyl-induced damage and is positively implicated in agronomically important seed traits. *Plant J.* **119**, 413–431 (2024).

26. Kamble, N. U., Petla, B. P., Ghosh, S., Achary, R. K. & Majee, M. Oryza coarctata PROTEIN L-

ISOASPARTYL METHYLTRANSFERASE (PIMT) repairs isoaspartyl modification to antioxidative enzymes and is implicated in seed traits in rice. *Environ. Exp. Bot.* **202**, 105027 (2022).

27. Achary, R. K. *et al.* The rice heat shock transcription factor OsHSFC1b increases seed weight, size, and vigor, but its function is disrupted by isoaspartyl modification. *Plant J.* **123**, 1–21 (2025).

28. Ghosh, S. *et al.* Arabidopsis protein l-ISOASPARTYL METHYLTRANSFERASE repairs isoaspartyl damage to antioxidant enzymes and increases heat and oxidative stress tolerance. *J. Biol. Chem.* **295**, 783–799 (2020).

29. Ghosh, S., Kamble, N. U. & Majee, M. A protein repairing enzyme, PROTEIN L-ISOASPARTYL METHYLTRANSFERASE is involved in salinity stress tolerance by increasing efficiency of ROS-scavenging enzymes. *Environ. Exp. Bot.* **180**, 104266 (2020).

30. Kamble, N. U., Ghosh, S., Achary, R. K. & Majee, M. Arabidopsis ABSCISIC ACID INSENSITIVE4 targets PROTEIN L-ISOASPARTYL METHYLTRANSFERASE1 in seed. *Planta 2022 2562* **256**, 1–8 (2022).

31. Zhao, C. J. *et al.* Identification of defense-related genes in rice responding to challenge by Rhizoctonia solani. *Theor. Appl. Genet.* **116**, 501–516 (2008).

32. Mendes-Giannini, M. J. S., Soares, C. P., Da Silva, J. L. M. & Andreotti, P. F. Interaction of pathogenic fungi with host cells: Molecular and cellular approaches. *FEMS Immunol. Med. Microbiol.* **45**, 383–394 (2005).

33. Yang, X. *et al.* Gene expression analysis of resistant and susceptible rice cultivars to sheath blight after inoculation with Rhizoctonia solani. *BMC Genomics 2022 231* **23**, 1–16 (2022).

34. Datta, K. *et al.* Over-expression of the cloned rice thaumatin-like protein (PR-5) gene in transgenic

rice plants enhances environmental friendly resistance to Rhizoctonia solani causing sheath blight disease. *Theor. Appl. Genet.* **98**, 1138–1145 (1999).

35. Ghosh, S., Kanwar, P. & Jha, G. Alterations in rice chloroplast integrity, photosynthesis and metabolome associated with pathogenesis of Rhizoctonia solani. *Sci. Reports 2017 71* **7**, 1–12 (2017).

36. Kant, R., Tyagi, K., Ghosh, S. & Jha, G. Host Alternative NADH:Ubiquinone Oxidoreductase Serves as a Susceptibility Factor to Promote Pathogenesis of Rhizoctonia solani in Plants. *https://doi.org/10.1094/PHYTO-02-19-0055-R* **109**, 1741–1750 (2019).

37. Morales, M. & Munné-Bosch, S. Malondialdehyde: Facts and Artifacts. *Plant Physiol.* **180**, 1246–1250 (2019).

38. Zhou, Q. *et al.* Effects of Different Drought Degrees on Physiological Characteristics and Endogenous Hormones of Soybean. *Plants 2022, Vol. 11, Page 2282* **11**, 2282 (2022).

39. Sunkar, R., Bartels, D. & Kirch, H. H. Overexpression of a stress-inducible aldehyde dehydrogenase gene from Arabidopsis thaliana in transgenic plants improves stress tolerance. *Plant J.* **35**, 452–464 (2003).

40. Shin, J. H., Kim, S. R. & An, G. Rice Aldehyde Dehydrogenase7 Is Needed for Seed Maturation and Viability. *Plant Physiol.* **149**, 905–915 (2009).

41. Huang, L. F. *et al.* Multiple Patterns of Regulation and Overexpression of a Ribonuclease-Like Pathogenesis-Related Protein Gene, OsPR10a, Conferring Disease Resistance in Rice and Arabidopsis. *PLoS One* **11**, e0156414 (2016).

42. Ersong, Z. *et al.* Regulation of OsPR10a Promoter Activity by Phytohormone and Pathogen Stimulation in Rice. *Rice Sci.* **28**, 442–456 (2021).

43. Tsuji, H., Tsutsumi, N., Sasaki, T., Hirai, A. & Nakazono, M. Organ-specific expressions and chromosomal locations of two mitochondrial aldehyde dehydrogenase genes from rice (Oryza sativa L.), ALDH2a and ALDH2b. *Gene* **305**, 195–204 (2003).

44. Lopes, N. dos S., Santos, A. S., de Novais, D. P. S., Pirovani, C. P. & Micheli, F. Pathogenesis-related protein 10 in resistance to biotic stress: progress in elucidating functions, regulation and modes of action. *Front. Plant Sci.* **14**, (2023).

45. Voigt, C. A., Schäfer, W. & Salomon, S. A comprehensive view on organ-specific callose synthesis in wheat (Triticum aestivum L.): glucan synthase-like gene expression, callose synthase activity, callose quantification and deposition. *Plant Physiol. Biochem.* **44**, 242–247 (2006).

46. Zhou, T., He, Y., Han, X., Sun, Q. & Xuan, Y. H. β-Glucanase Family Genes Promote Resistance to Sheath Blight in Rice by Inhibiting the Permeability of Plasmodesmata. *J. Agric. Food Chem.* **71**, 9667–9676 (2023).

47. Pradhan, A., Yadav, S. K. & Jha, G. Glycosyltransferase-Like Toxin of Burkholderia gladioli Strain NGJ1 Is a Potent Antifungal Protein with Potential for Control of Sheath Blight Disease in Rice. *https://doi.org/10.1094/PHYTO-12-24-0383-R* **115**, 485–494 (2025).

48. Georgiou, C. D., Patsoukis, N., Papapostolou, I. & Zervoudakis, G. Sclerotial metamorphosis in filamentous fungi is induced by oxidative stress. *Integr. Comp. Biol.* **46**, 691–712 (2006).

49. Foley, R. C., Kidd, B. N., Hane, J. K., Anderson, J. P. & Singh, K. B. Reactive Oxygen Species Play a Role in the Infection of the Necrotrophic Fungi, Rhizoctonia solani in Wheat. *PLoS One* **11**, e0152548 (2016).

50. Wang, C. *et al.* ROS and trehalose regulate sclerotial development in Rhizoctonia solani AG-1 IA. *Fungal Biol.* **122**, 322–332 (2018).

51. Samsatly, J., Copley, T. R. & Jabaji, S. H. Antioxidant genes of plants and fungal pathogens are distinctly regulated during disease development in different Rhizoctonia solani pathosystems. *PLoS One* **13**, e0192682 (2018).

52. Wang, R., Li, J. & Liang, Y. Role of ROS signaling in the plant defense against vascular pathogens. *Curr. Opin. Plant Biol.* **81**, 102617 (2024).

53. Fu, Z. *et al.* The effector AGLIP1 hijacks peroxidase OsAPX8 to coordinate rice immune suppression and ROS-Driven cell death for facilitating Rhizoctonia solani infection. *J. Adv. Res.* (2025) doi:10.1016/J.JARE.2025.10.063.

54. Penninckx, I. A. M. A., Thomma, B. P. H. J., Buchala, A., Métraux, J.-P. & Broekaert, W. F. Concomitant Activation of Jasmonate and Ethylene Response Pathways Is Required for Induction of a Plant Defensin Gene in Arabidopsis. *Plant Cell* **10**, 2103–2113 (1998).

55. Thomma, B. P. H. J., Eggermont, K., Broekaert, W. F. & Cammue, B. P. A. Disease development of several fungi on Arabidopsis can be reduced by treatment with methyl jasmonate. *Plant Physiol. Biochem.* **38**, 421–427 (2000).

56. Glazebrook, J. Contrasting mechanisms of defense against biotrophic and necrotrophic pathogens. *Annu. Rev. Phytopathol.* **43**, 205–227 (2005).

57. Rakwal, R., Agrawal, G. K. & Yonekura, M. Light-dependent induction of OsPR10 in rice (Oryza sativa L.) seedlings by the global stress signaling molecule jasmonic acid and protein phosphatase 2A inhibitors. *Plant Sci.* **161**, 469–479 (2001).

58. Nakazono, M. *et al.* Expression of a Gene Encoding Mitochondrial Aldehyde Dehydrogenase in Rice Increases under Submerged Conditions. *Plant Physiol.* **124**, 587 (2000).

59. Kotchoni, S. O., Kuhns, C., Ditzer, A., Kirch, H. H. & Bartels, D. Over-expression of different

aldehyde dehydrogenase genes in Arabidopsis thaliana confers tolerance to abiotic stress and protects plants against lipid peroxidation and oxidative stress. *Plant. Cell Environ.* **29**, 1033–1048 (2006).

60. Ke, Y. *et al.* The versatile functions of OsALDH2B1 provide a genic basis for growth–defense trade-offs in rice. *Proc. Natl. Acad. Sci. U. S. A.* **117**, 3867–3873 (2020).

61. Shen, Y. *et al.* Mutation of OsALDH7 causes a yellow-colored endosperm associated with accumulation of oryzamutaic acid A in rice. *Planta 2011 2352* **235**, 433–441 (2011).

62. Xie, K., Minkenberg, B. & Yang, Y. Boosting CRISPR/Cas9 multiplex editing capability with the endogenous tRNA-processing system. *Proc. Natl. Acad. Sci. U. S. A.* **112**, 3570–3575 (2015).

63. Francis, A. *et al.* Evolution of pathogenicity-associated genes in Rhizoctonia solani AG1-IA by genome duplication and transposon-mediated gene function alterations. *BMC Biol. 2023 211* **21**, 15- (2023).

64. Swain, D. M. *et al.* Concurrent overexpression of rice G-protein β and γ subunits provide enhanced tolerance to sheath blight disease and abiotic stress in rice. *Planta 2019 2505* **250**, 1505–1520 (2019).

65. Bradford, M. M. A rapid and sensitive method for the quantitation of microgram quantities of protein utilizing the principle of protein-dye binding. *Anal. Biochem.* **72**, 248–254 (1976).

66. Verma, P., Singh, A., Kaur, H. & Majee, M. PROTEIN l-ISOASPARTYL METHYLTRANSFERASE1 (CaPIMT1) from chickpea mitigates oxidative stress-induced growth inhibition of Escherichia coli. *Planta 2009 2312* **231**, 329–336 (2009).

67. Varshney, V. *et al.* The Arabidopsis F-box protein SKP1-INTERACTING PARTNER 31 modulates seed maturation and seed vigor by targeting JASMONATE ZIM DOMAIN proteins

independently of jasmonic acid-isoleucine. *Plant Cell* **35**, 3712–3738 (2023).

68. Ghosh, S., Kant, R., Pradhan, A. & Jha, G. RS_CRZ1, a C2H2-Type Transcription Factor Is Required for Pathogenesis of Rhizoctonia solani AG1-IA in Tomato. *https://doi.org/10.1094/MPMI-05-20-0121-R* **34**, 26–38 (2020).

69. Uttam Kamble, N. *et al.* Initiation of B-type starch granules in wheat endosperm requires the plastidial α-glucan phosphorylase PHS1. *Plant Cell* **35**, 4091–4110 (2023).

70. Hazra, A. *et al.* Methionine sulfoxide reductase B5 plays a key role in preserving seed vigor and longevity in rice (Oryza sativa). *New Phytol.* **236**, 1042–1060 (2022).

71. Tyagi, K. *et al.* The host and pathogen myo-inositol-1-phosphate synthases are required for Rhizoctonia solani AG1-IA infection in tomato. *Mol. Plant Pathol.* **25**, e13470 (2024).

72. Heath, R. L. & Packer, L. Photoperoxidation in isolated chloroplasts: I. Kinetics and stoichiometry of fatty acid peroxidation. *Arch. Biochem. Biophys.* **125**, 189–198 (1968).

73. Alexieva, V., Sergiev, I., Mapelli, S. & Karanov, E. The effect of drought and ultraviolet radiation on growth and stress markers in pea and wheat. *Plant, Cell Environ.* **24**, 1337–1344 (2001).

74. Salvi, P. *et al.* Differentially expressed galactinol synthase(s) in chickpea are implicated in seed vigor and longevity by limiting the age induced ROS accumulation. *Sci. Rep.* **6**, 1–15 (2016).

75. Weydert, C. J. & Cullen, J. J. Measurement of superoxide dismutase, catalase and glutathione peroxidase in cultured cells and tissue. *Nat. Protoc.* **5**, 51–66 (2010).

76. Elavarthi, S. & Martin, B. Spectrophotometric assays for antioxidant enzymes in plants. *Methods Mol. Biol.* **639**, 273–281 (2010).

77. Vadassery, J. *et al.* CML42-Mediated Calcium Signaling Coordinates Responses to Spodoptera

Herbivory and Abiotic Stresses in Arabidopsis. *Plant Physiol.* **159**, 1159–1175 (2012).

78. Rao, V. *et al.* Arabidopsis SKP1-like protein13 (ASK13) positively regulates seed germination and seedling growth under abiotic stress. *J. Exp. Bot.* **69**, 3899–3915 (2018).

79. Chandan, R. K. *et al.* RAV1 family members function as transcriptional regulators and play a positive role in plant disease resistance. *Plant J.* **114**, 39–54 (2023).

Acknowledgements

We thank the BRIC-NIPGR metabolome facility and proteomic facility [DBT grant (no. BT/INF/22/SP28268/2018)], confocal microscopy facility, radioisotope facility and central instrumentation facility. We thank the technicians Ms. Umamaheswari Rajamani and Shri Naga Vara Prasad G of NIPGR proteomic facility for assisting MS/MS analysis and data submission. GJ acknowledges SR-NBACD award (HRD-20/3/2024-HRD-DBT), Swarna Jayanti Fellowship (SB/SJF/2020-21/01; ANRF (SERB)-funded), CRG grant (CRG/2022/004092, ANRF (SERB)-funded) and BRIC-NIPGR core research grant. NUK acknowledges Indian Institute of Science Education and Research, Thiruvananthapuram core research grant. R.K.C. acknowledges financial support from the DBT-RA programme in Biotechnology and Life Sciences. The authors are thankful to DBT-eLibrary Consortium (DeLCON) for providing access to e-resources.

Funding Statement

This work was supported by grant from the Department of Biotechnology, Government of India (BT/NIPGR/Flagship-prog/2018-19) and a core grant to MM from the BRIC-National Institute of Plant Genome Research. All authors gratefully thank the Council of Scientific and Industrial Research, University Grant Commission, Department of Biotechnology, Government of India, and BRIC-National Institute of Plant Genome Research for research fellowships.

Author Contributions

S.G., N.U.K., and M.M. conceived the idea and designed the research. S.G. and N.U.K. performed the experiments, analyzed data and prepared figures. R.K.C. and G.J. guided and helped with pathogenesis experiments. R.K.A., V.V., A.H., S.L., S.M., So.M, and S.S. helped with experiments, plant growth and sample collection. S.G., N.U.K., and M.M. wrote the manuscript with inputs from all the authors. All authors read and approved the final version of the manuscript. M.M. agrees to serve as the author responsible for contact and ensuring communication.

Competing Interests

The authors declare no competing interests.

FIGURE LEGENDS

Fig. 1. isoAsp accumulation and *PIMT*s are induced upon *R. solani* infection in rice. (**a**) 3, 3′-diaminobenzidine (DAB), Nitroblue tetrazolium (NBT), and Trypan blue (Trypan blue) staining of *R. solani* infected sheaths collected from control and infected plants at different time points (dpi), scale bar=1cm. (**b, c**) Quantification of (**b**) isoAsp accumulation, (**c**) PIMT enzymatic activity. (**d**, **e**) Expression levels of (**d**) *OsPIMT1* and (**e**) *OsPIMT2* normalized to rice *OsUBQ10* using RT-qPCR. (**f**) PIMT protein accumulation by Western blot analysis using anti-PIMT antibodies (top panel) and anti-tubulin antibodies (lower panel). Values below the panel denote the normalized values of PIMT protein accumulation quantified using ImageJ, with tubulin as the internal control. For (b), (c) and (f), 50µg of crude protein extracts of *R. solani* infected sheaths was used. In a, and f, each experiment was independently repeated three times with similar results, and representative data are shown. In b-e, data represent means ±SE of three biological replicates. Different letters indicate significant differences (one-way ANOVA followed by Tukey's post hoc test, $P < 0.05$, for exact P-values, see Source Data).

Fig. 2. Overexpression of *OsPIMT*s enhances tolerance to *R. solani* infection and restricts fungal penetration. (**a**) Infection phenotypes of WT, *OsPIMT1:OE*, *OsPIMT2:OE*, and *OsPIMT:RNAi* lines infected with *R. solani* at 3 dpi. Scale bar=1cm. (**b, c**) Quantification of (**b**) Disease index calculated based on relative vertical sheath colonization (RVSC) index; (**c**) Disease lesion length. (**d**) Fungal pathogen load measured as the relative abundance of *R. solani 18S rRNA* normalized to rice *17S rRNA* using RT-qPCR. (**e**) Three-dimensional confocal imaging of *R. solani* penetration in infected leaf sheaths, stained with WGA-FITC (Wheat germ agglutinin coupled with FITC). The z-axis indicates penetration depth, represented by the color index bars. Scale bar=200µm. (**f**) Quantification of penetration depth for (e) Analysis of the maximal depth achieved by fungal hyphae penetrating the infected leaf sheaths. (**g**) isoAsp quantification in control and *R. solani* infected sheaths. For (c) The disease lesion length was assessed using ImageJ software. In a, and e, each experiment was independently repeated three times with similar results, and representative data are shown. In b-d and f-g, data represent means ±SE of three biological replicates. Different letters indicate significant differences (one-way ANOVA followed by Tukey's post hoc test, $P < 0.05$, for exact P-values, see Source Data).

Fig. 3. *OsPIMTs* maintains ROS homeostasis, decreases cell death, and enhances tolerance to *R. solani* infection. (**a**) Representative confocal micrographs of H_2DCFDA-stained sheaths from WT, *OsPIMT1:OE*, *OsPIMT2:OE*, and *OsPIMT:RNAi* lines infected with *R. solani*. Scale bar=20μm. (**b**) Sheaths of WT, *OsPIMT1:OE*, *OsPIMT2:OE*, and *OsPIMT:RNAi* lines stained with 3, 3′-diaminobenzidine (DAB) top panel and Trypan blue lower panel. For (b) top and lower panel Scale bar=1cm. Quantification of (**c**) H_2O_2 and **(d)** Malondialdehyde (MDA) accumulation. (**e**, **f**) Quantification of antioxidant enzymes activity **(e)** Catalase (CAT) **(f)** Ascorbate peroxidases (APX) upon *R. solani* infection. In a, and b, each experiment was independently repeated three times with similar results, and representative data are shown. In c-f, data represent means ±SE of three biological replicates. Different letters indicate significant differences (one-way ANOVA followed by Tukey's post hoc test, $P < 0.05$, for exact P-values, see Source Data).

Fig. 4. *pimt* mutants exhibit hypersensitivity to *R. solani* infection. (**a**, **b**) Identification of genome edited lines of *OsPIMT1* and *OsPIMT2* generated via CRISPR/Cas9 using Sanger sequencing. (**c**) Infection phenotypes of WT, *pimt1*, and *pimt2* mutant lines infected with *R. solani* at 3dpi. Scale bar=1cm. (**d**, **e**) Quantification of (**d**) Disease index calculated based on relative vertical sheath colonization (RVSC) index; (**e**) Disease lesion length. (**f**) isoAsp quantification in control, and *R. solani* infected sheaths. (**g**) Fungal pathogen load measured as the relative abundance of *R. solani 18S rRNA* normalized to rice *17S rRNA* using RT-qPCR. (**h**) Three-dimensional confocal imaging of *R. solani* penetration in infected leaf sheaths, stained with WGA-FITC. The z-axis indicates penetration depth, represented by the color index bars. Scale bar=200μm. (**i**) Quantification of penetration depth for (**j**). Analysis of the maximal depth achieved by fungal hyphae penetrating the infected leaf sheaths. For (e) the disease lesion length was assessed using ImageJ software. In c and h, each experiment was independently repeated three times with similar results, and representative data are shown. In d to i, data represent means ±SE of three biological replicates. Different letters indicate significant differences (one-way ANOVA followed by Tukey's post hoc test, $P < 0.05$, for exact P-values, see Source Data).

Fig. 5. *pimt* mutants show dysregulated ROS homeostasis, accelerated cell death, and increased susceptibility to *R. solani* infection. (**a**) Representative confocal micrographs of H_2DCFDA-stained sheaths from WT, *pimt1*, and *pimt2* mutant lines infected with *R. solani*. Scale bar=20μm. (**b**) Sheaths from WT, *pimt1*, and *pimt2* mutant lines stained with 3, 3′-diaminobenzidine (DAB) top panel and Trypan blue lower panel. For (b) top and lower panel Scale bar=1cm. (**c**) Quantification of H_2O_2 accumulation and **(d)** Malondialdehyde (MDA) accumulation. (**e**, **f**) Quantification of antioxidant enzymes activities **(e)** Catalase and **(f)** Ascorbate peroxidases upon *R. solani* infection. In a, and b, each experiment was independently repeated three times with similar results, and representative data are shown. In c-f, data represent means ±SE of three biological replicates. Different letters indicate significant differences (one-way ANOVA followed by Tukey's post hoc test, $P < 0.05$, for exact P-values, see Source Data).

Fig. 6. PIMT1 restores compromised catalytic activity of OsALDH and OsPBZ1 due to isoAsp accumulation. (**a, b**) SDS-PAGE analysis of recombinant purified proteins, (**a**) OsALDH and (**b**) OsPBZ1. (**c, d**) isoAsp accumulation in recombinant proteins before and after H_2O_2 treatment at 25°C, (**c**) OsALDH, **(d**) OsPBZ1. (**e, f**) ESI mass spectra for tryptic peptides of immunoprecipitated proteins from infected sheaths identified using MS/MS, **(e)** OsALDH, **(f)** OsPBZ1. (**g, h**) isoAsp accumulation in recombinant purified untreated, treated, and repaired proteins, **(g)** OsALDH and **(h)** OsPBZ1. (**i, j**) Enzymatic activity in recombinant purified untreated, treated, and repaired proteins as in (g, h), **(i)** OsALDH and **(j)** OsPBZ1.

Recombinant purified OsALDH or OsPBZ1 protein were treated with H_2O_2 and repaired with eighter OsPIMT1 (biochemically active) or OcPIMT1-2 (biochemically inactive). Following the PIMT repair assay, isoAsp accumulation (**g, h**) and enzymatic activity (**i, j**) was determined; (+) and (-) indicate the presence and absence of active or inactive PIMT protein, respectively. For (e and f) Fragment ion series (y- and b-ions) were assigned using ProteinPilot software, version 5.0.1. Sites of deamidation are indicated in square brackets within peptide sequences [Dea]. In a-b, and e-f, each experiment was independently repeated three and two times respectively with similar results, and representative data are shown. In c-d, and g-j, data represent means ±SE of three biological replicates. Asterisk and different letters indicate significant differences [Student T-test (**P = 0.01, *P = 0.05) and one-way ANOVA followed by Tukey's post hoc test, $P < 0.05$, respectively for exact P-values, see Source Data].

Fig. 7. OsPIMTs physically interact with OsALDH and OsPBZ1. (**a**) Yeast two-hybrid (Y2H) assay showing interactions between OsPIMTs and OsALDH or OsPBZ1. Cells were plated on a SD-Leu-Trp (DDO) or SD-Ade-Leu-Trp-His (QDO) alone or supplemented with X-α-Gal and Aureobasidin A to analyse the interaction. PC, positive control; NC, negative control. (**b**) Bimolecular fluorescence complementation (BiFC) analysis in *N. benthamiana*. OsPIMTs were fused to the N-terminal fragment of YFP (nYFP), and OsALDH or OsPBZ1were fused to the C-terminal fragment of YFP (cYFP). Images were captured by confocal microscopy OsALDH (left panel) and OsPBZ1 (right panel). The relevant negative controls showed no fluorescence. Channels shown: YFP fluorescence, RFP fluorescence, bright field (BF), and merged images. The experiments were repeated independently with similar results at least 3 times. Scale bar=20μm. Pairwise immunoprecipitation using (**c**) *in-vitro* and **(d)** *in-vivo* immunoprecipitation assay showing interaction between OsPIMT1 and OsALDH [left panels in (c) and (d)] or OsPBZ1 [right panels in (c) and (d)]. For (c), pulldown experiment was performed with the anti-GST antibody. Input and IP samples were immunoblotted with anti-GST and anti-MBP antibodies. For (d). OsPIMT1 and OsALDH or OsPBZ1 co-expressed in *N. benthamiana* leaves. Pulldown was performed with the anti-Myc antibody. Input and IP samples were immunoblotted with anti-Myc and anti-PIMT antibodies. In a-d, each experiment was independently repeated two -three times respectively with similar results, and representative data are shown.

Fig. 8. Overexpression of *OsALDH* reduces ROS accumulation, decreases cell death, and enhances tolerance to *R. solani* infection. (**a, b**) Relative transcript accumulation of (**a**) *OsALDH* and (**b**) *OsPBZ1*. WT and *pimt1* mutant lines transiently transformed with either a vector control (VC) or the *OsALDH* overexpression construct. Samples were harvested before and after *R. solani* infection at 3dpi and used for the quantification or disease phenotypes. (**c**) Relative transcript accumulation of *OsALDH*. (**d**) Disease phenotypes of infected plants. Scale bar=1cm. (**e**) Disease index calculated based on relative vertical sheath colonization (RVSC) index. (**f**) Fungal pathogen load measured as the relative abundance of *R. solani 18S rRNA* normalized to rice *17S rRNA* using qRT-PCR. (**g**) Quantification of isoAsp accumulation in Myc tagged OsALDH immunoprecipitated using anti-Myc antibodies from WT and *pimt1* plants infected with *R. solani*. (**h**) Confocal microscopy images depicting reduced *R. solani* penetration in sheaths overexpressing *OsALDH*. Samples were stained with WGA-FITC. Three-dimensional reconstruction shows fungal invasion depth, with the Z-axis represented by color index bars. Scale bar=200μm. (**i**) Quantification of fungal penetration depth in infected leaf sheaths. (**j**) Histochemical detection of ROS by DAB staining and (**k**) Cell death by Trypan blue staining. Quantification of (**l**) H_2O_2 content and (**m**) malondialdehyde (MDA) content after *R. solani* infection. In (h) samples were stained with WGA-FITC (Wheat germ agglutinin coupled with FITC). The z-axis indicates penetration depth, represented by the color index bars. In d, h and j-k, each experiment was independently repeated three times with similar results, and representative data are shown. In a-c, e-i, and l-m, data represent means ±SE of three biological

replicates. Different letters indicate significant differences (one-way ANOVA followed by Tukey's post hoc test, $P < 0.05$, for exact P-values, see Source Data).

Fig. 9. OsALDH (or OsPBZ1) inhibits fungal proliferation by reducing ROS and disrupting mycelial morphology in *R. solani* hyphae which requires PIMT-mediated repair. (**a**) Anti-fungal plate assay showing restricted *R. solani* fungal growth in sclerotia treated with either purified OsALDH (or OsPBZ1) [Control], H_2O_2 treated OsALDH (or OsPBZ1) [Treated] and H_2O_2 treated OsALDH (or OsPBZ1) repaired by OsPIMT1 [Repaired]. OsALDH (right panel) and OsPBZ1 (left panel). 20µg/µl purified OsALDH (or OsPBZ1) was used for sclerotia treatment and treated sclerotia were allowed to germinate on PDA plates. Plates were imaged at 2dpi (top panel) and 4dpi (bottom panel). Scale bar =1cm. (**b**, **c**) Quantification of radial diameter of fungal growth for plates shown in (a), (**b**) OsALDH (**c**) OsPBZ1. (**d**) Representative confocal micrographs of H_2DCFDA stained *R. solani* hyphae from plates shown in (a), H_2O_2 treated hyphae (as positive control). (**e**) Mean gray value quantification by ImageJ for confocal images of stained fungus shown in (d). (**f**) Representative scanning electron micrographs of *R. solani* hyphae from plates shown in (a). Arrow indicates hyphal deformities. Scale bars represent 50µm in (d) and 20µm in (e). Part of panel in a is Created in BioRender. Majee, M. (2026) https://BioRender.com/2it733v. In a, d and f, each experiment was independently repeated three times with similar results, and representative data are shown. In b-c and e, data represent means ±SE of three biological replicates. Different letters indicate significant differences (one-way ANOVA followed by Tukey's post hoc test, $P < 0.05$, for exact P-values, see Source Data).

Fig. 10. A working model depicting the role of PIMT in rice sheath blight disease tolerance. *R. solani* infection induces the expression of PIMT to restrict the isoAsp and ROS accumulation by maintaining the enzymatic activity of different antioxidant enzymes as well as OsALDH and OsPBZ1 (Left panel). In contrast, *R. solani* infection in OsPIMT mutant plants leads to the conversion of asparagine (Asn) and aspartic acid (Asp) residues in antioxidant proteins, OsALDH, and OsPBZ1 into isoaspartates (isoAsp), thereby reducing their enzymatic activities and compromised tolerance. Part of figure is Created in BioRender. Majee, M. (2026) https://BioRender.com/b3005yi

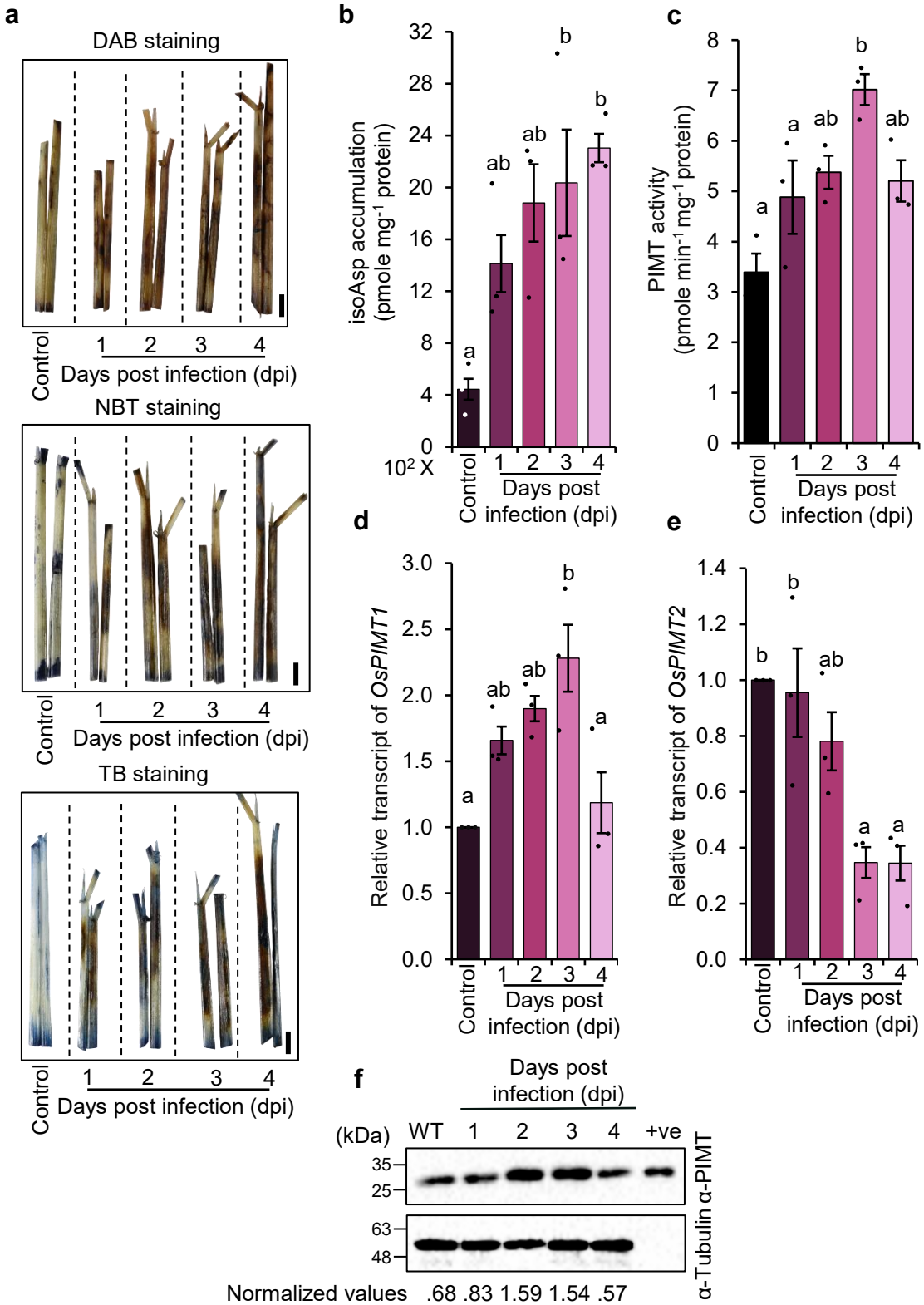
a
DAB staining
Control
1 2 3 4
Days post infection (dpi)
NBT staining
Control
1 2 3 4
Days post infection (dpi)
TB staining
Control
1 2 3 4
Days post infection (dpi)
b
isoAsp accumulation (pmole mg-1 protein)
10² X
Control
1 2 3 4
Days post infection (dpi)
c
PIMT activity (pmole min-1 mg-1 protein)
Control
1 2 3 4
Days post infection (dpi)
d
Relative transcript of OsPIMT1
Control
1 2 3 4
Days post infection (dpi)
e
Relative transcript of OsPIMT2
Control
1 2 3 4
Days post infection (dpi)
f
Days post infection (dpi)
(kDa) WT 1 2 3 4 +ve
35
25
63
48
α-PIMT
α-Tubulin
Normalized values .68 .83 1.59 1.54 .57

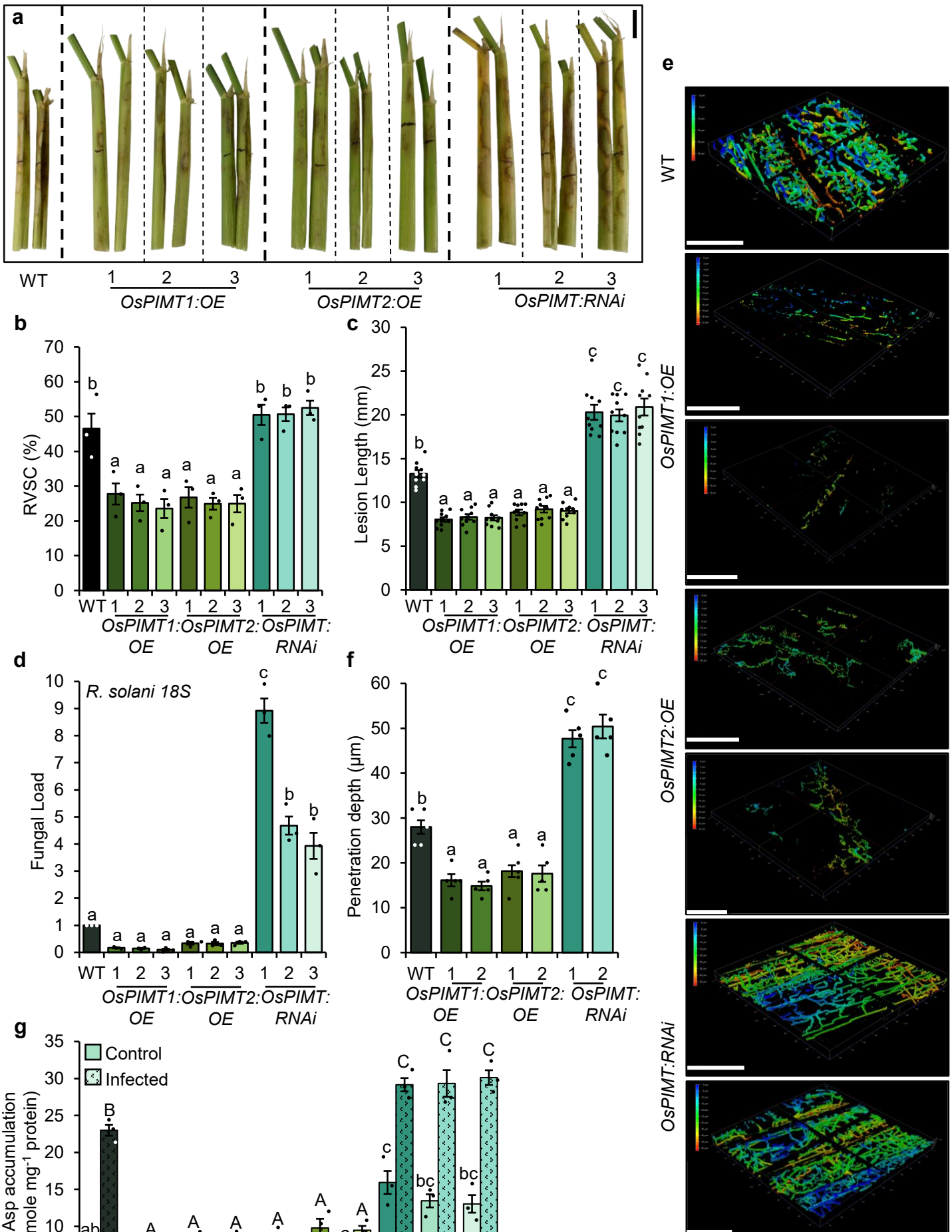
a
WT
1 2 3
OsPIMT1:OE
1 2 3
OsPIMT2:OE
1 2 3
OsPIMT:RNAi
b
RVSC (%)
WT 1 2 3 1 2 3 1 2 3
OsPIMT1: OE
OsPIMT2: OE
OsPIMT: RNAi
c
Lesion Length (mm)
WT 1 2 3 1 2 3 1 2 3
OsPIMT1: OE
OsPIMT2: OE
OsPIMT: RNAi
d
R. solani 18S
Fungal Load
WT 1 2 3 1 2 3 1 2 3
OsPIMT1: OE
OsPIMT2: OE
OsPIMT: RNAi
f
Penetration depth (µm)
WT 1 2 1 2 1 2
OsPIMT1: OE
OsPIMT2: OE
OsPIMT: RNAi
g
Control
Infected
isoAsp accumulation (pmole mg-1 protein)
10² X
WT 1 2 3 1 2 3 1 2 3
OsPIMT1:OE
OsPIMT2:OE
OsPIMT:RNAi
e
WT
OsPIMT1:OE
OsPIMT2:OE
OsPIMT:RNAi

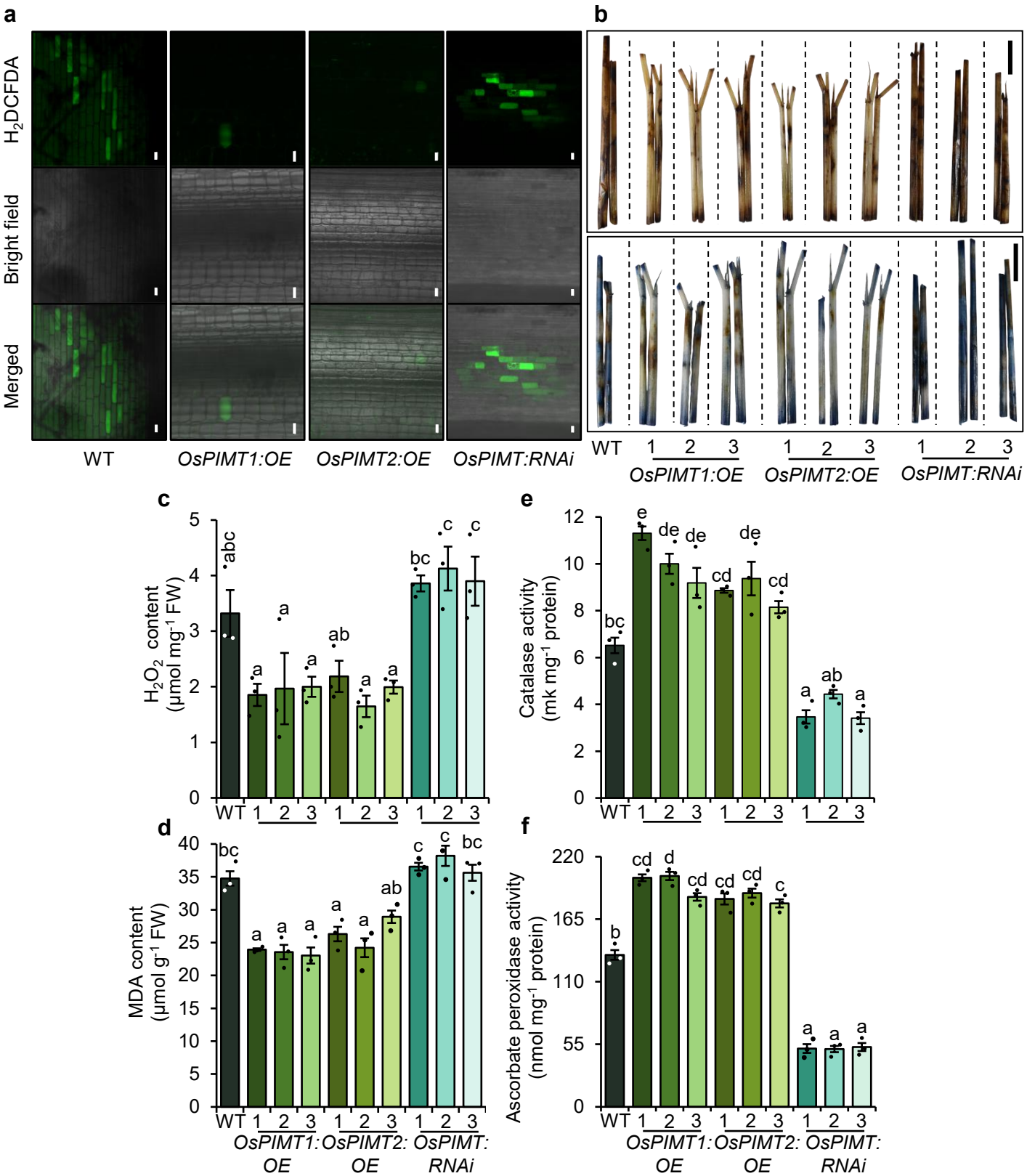
a
H2DCFDA
Bright field
Merged
WT
OsPIMT1:OE
OsPIMT2:OE
OsPIMT:RNAi
b
WT
1 2 3
OsPIMT1:OE
OsPIMT2:OE
OsPIMT:RNAi
c
H2O2 content (µmol mg-1 FW)
d
MDA content (µmol g-1 FW)
e
Catalase activity (mk mg-1 protein)
f
Ascorbate peroxidase activity (nmol mg-1 protein)
OsPIMT1: OE
OsPIMT2: OE
OsPIMT: RNAi

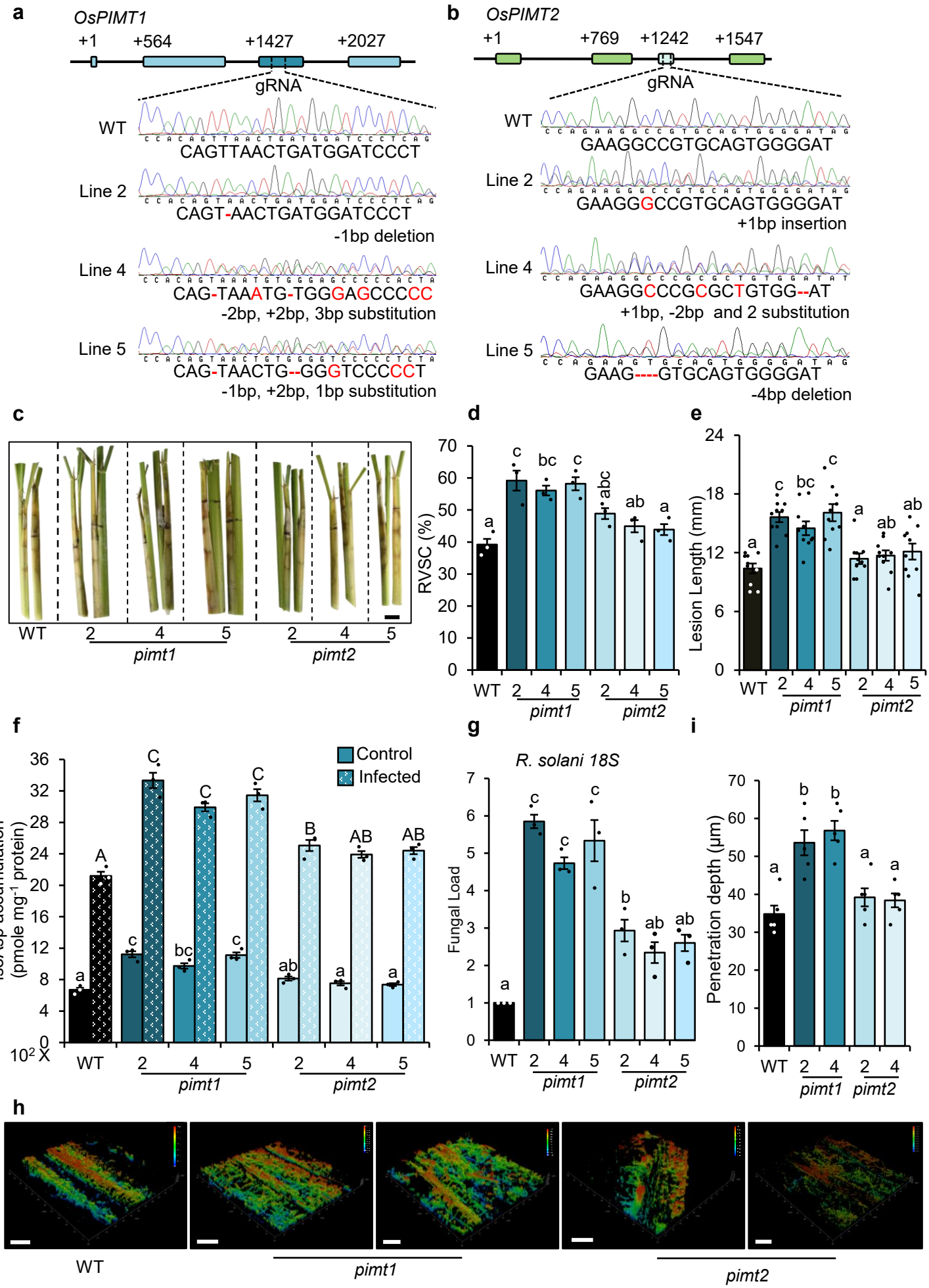
a
OsPIMT1
+1
+564
+1427
+2027
gRNA
WT
CAGTTAACTGATGGATCCCT
Line 2
CAGT-AACTGATGGATCCCT
-1bp deletion
Line 4
CAG-TAAATG-TGGGAGCCCCC
-2bp, +2bp, 3bp substitution
Line 5
CAG-TAACTG--GGGTCCCCCT
-1bp, +2bp, 1bp substitution
b
OsPIMT2
+1
+769
+1242
+1547
gRNA
WT
GAAGGCCGTGCAGTGGGGAT
Line 2
GAAGGGCCGTGCAGTGGGGAT
+1bp insertion
Line 4
GAAGGCCCGCGCTGTGG--AT
+1bp, -2bp and 2 substitution
Line 5
GAAG----GTGCAGTGGGGAT
-4bp deletion
c
WT
2
4
5
pimt1
pimt2
d
RVSC (%)
e
Lesion Length (mm)
f
Control
Infected
isoAsp accumulation (pmole mg-1 protein)
10² X
g
R. solani 18S
Fungal Load
i
Penetration depth (µm)
h
WT
pimt1
pimt2

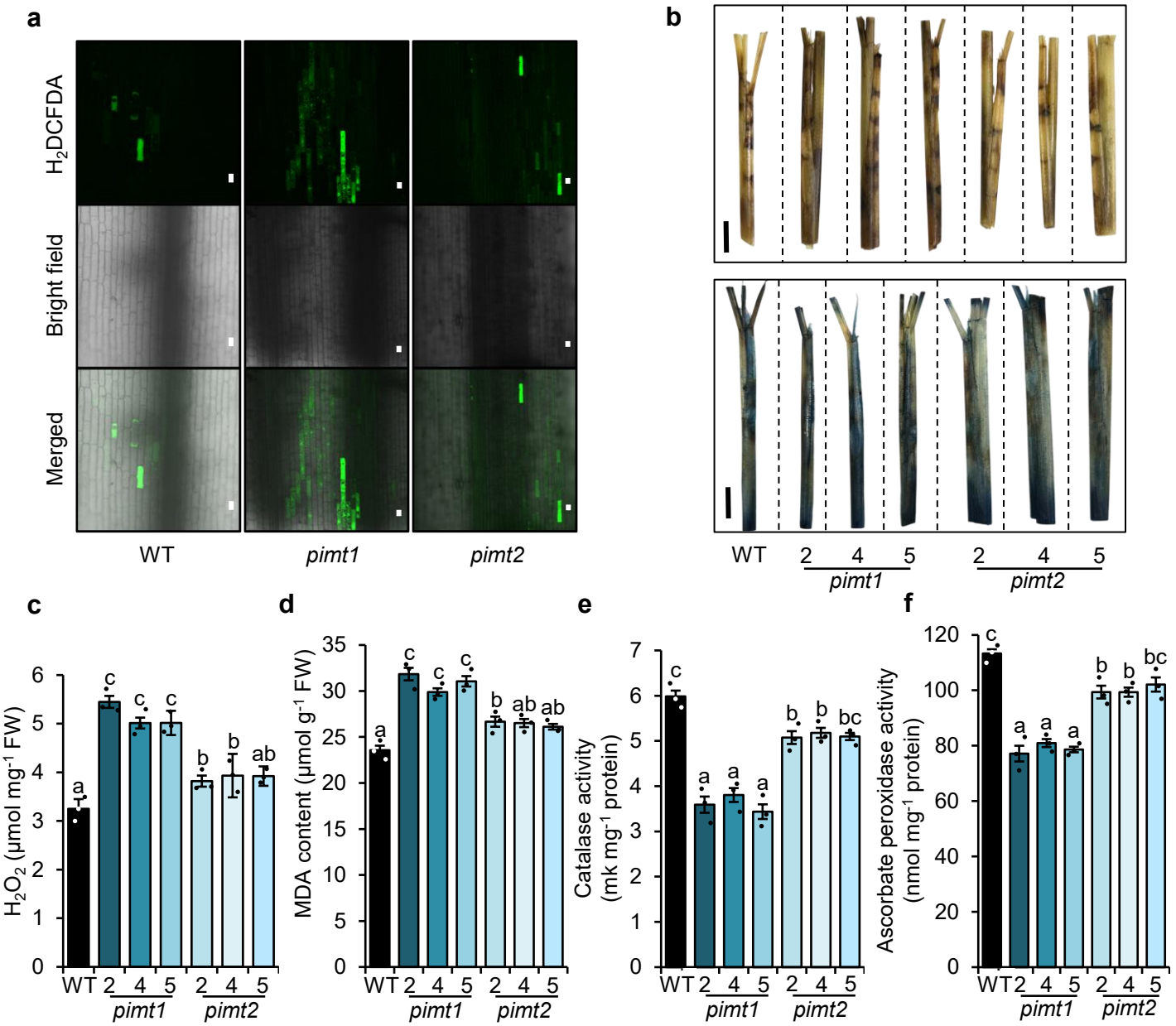
a
H2DCFDA
Bright field
Merged
WT
pimt1
pimt2
b
WT
2 4 5
pimt1
2 4 5
pimt2
c
H2O2 (μmol mg-1 FW)
d
MDA content (μmol g-1 FW)
e
Catalase activity (mk mg-1 protein)
f
Ascorbate peroxidase activity (nmol mg-1 protein)

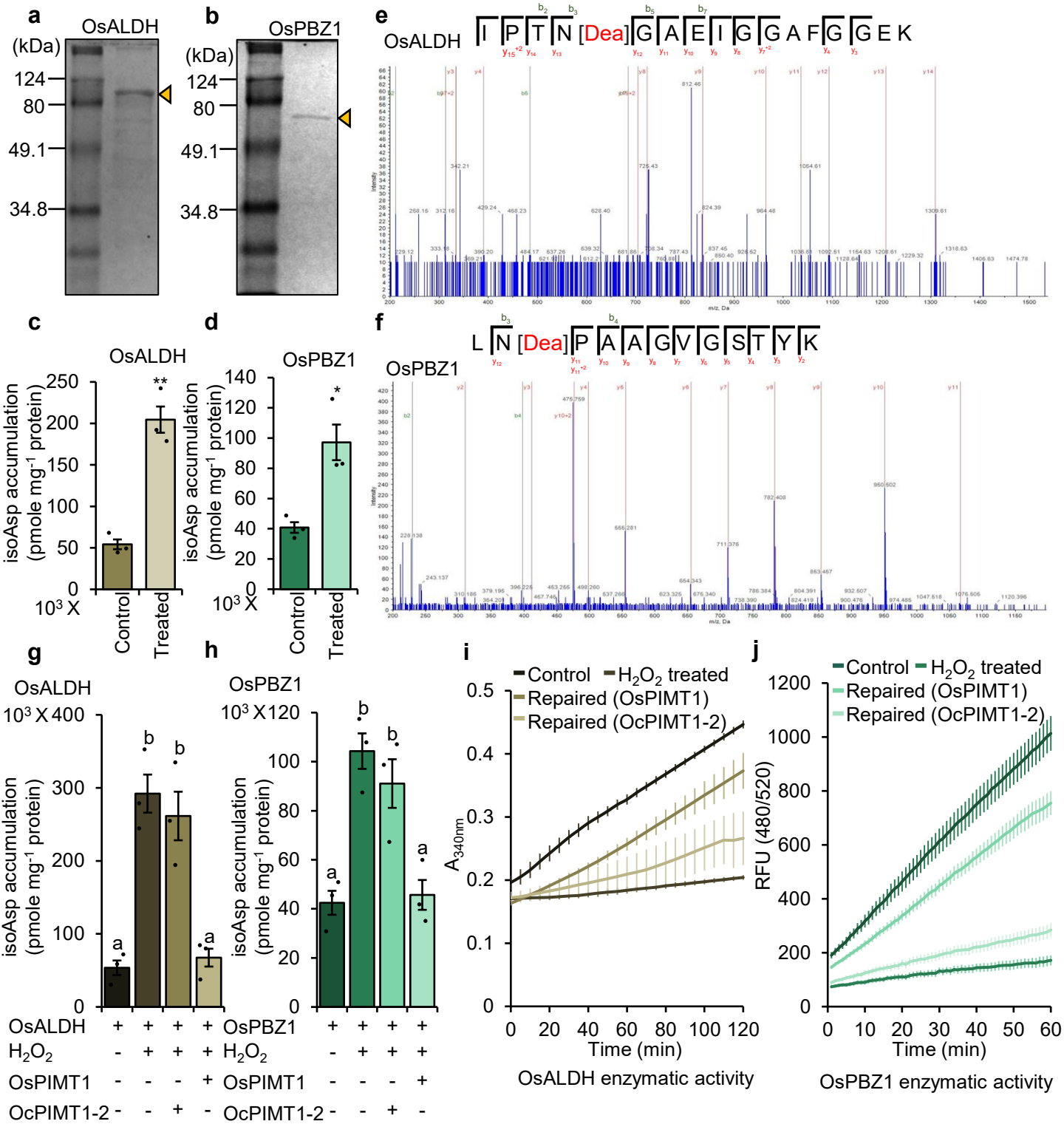
a
OsALDH
(kDa)
124
80
49.1
34.8
b
OsPBZ1
(kDa)
124
80
49.1
34.8
e
OsALDH
I P T N [Dea] G A E I G G A F G G E K
c
OsALDH
isoAsp accumulation (pmole mg-1 protein)
10³ X
Control
Treated
d
OsPBZ1
isoAsp accumulation (pmole mg-1 protein)
10³ X
Control
Treated
f
OsPBZ1
L N [Dea] P A A G V G S T Y K
g
OsALDH
10³ X
isoAsp accumulation (pmole mg-1 protein)
OsALDH + + + +
H2O2 - + + +
OsPIMT1 - - - +
OcPIMT1-2 - - + -
h
OsPBZ1
10³ X
isoAsp accumulation (pmole mg-1 protein)
OsPBZ1 + + + +
H2O2 - + + +
OsPIMT1 - - - +
OcPIMT1-2 - - + -
i
Control
H2O2 treated
Repaired (OsPIMT1)
Repaired (OcPIMT1-2)
A340nm
Time (min)
OsALDH enzymatic activity
j
Control
H2O2 treated
Repaired (OsPIMT1)
Repaired (OcPIMT1-2)
RFU (480/520)
Time (min)
OsPBZ1 enzymatic activity

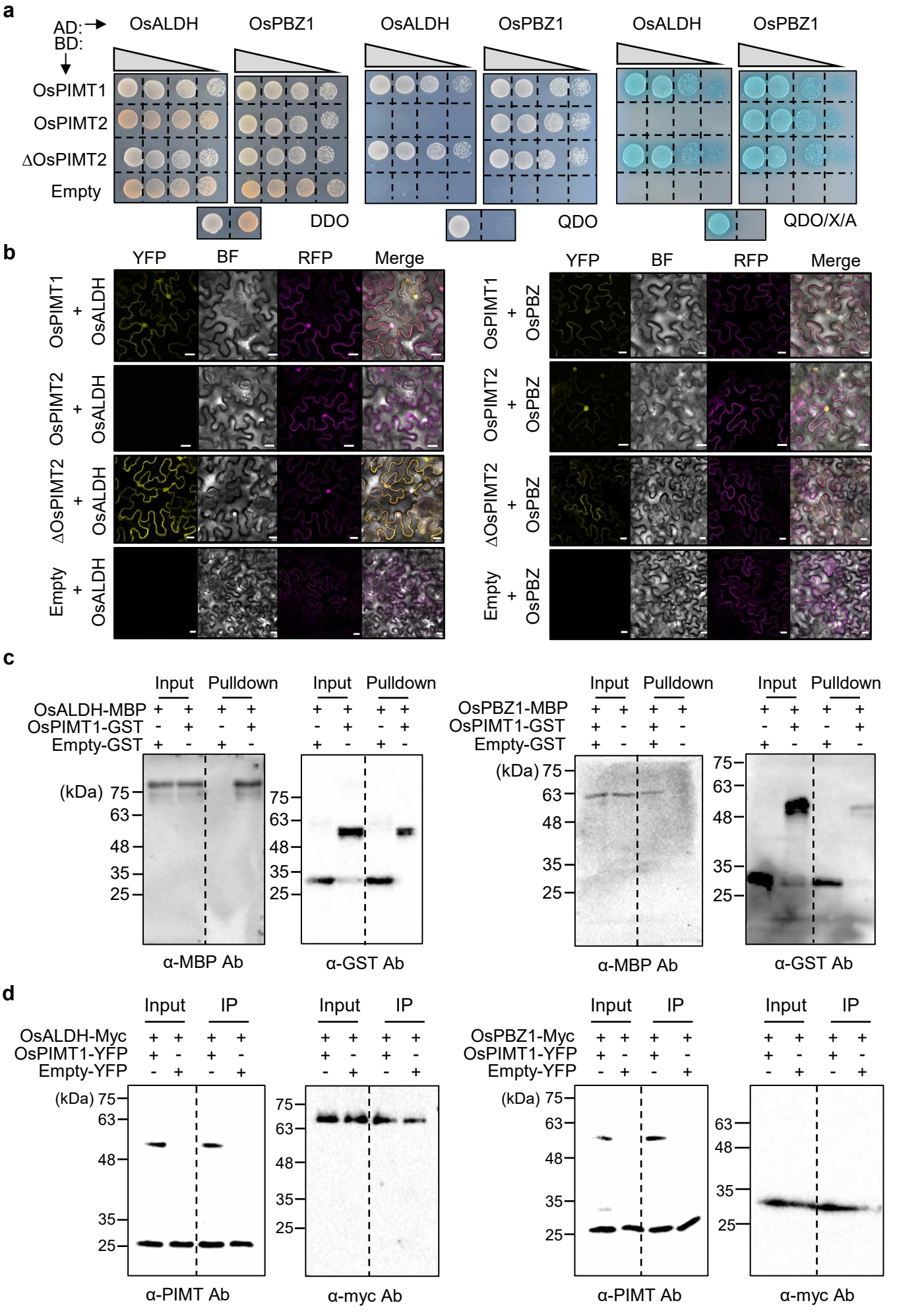
a
AD:
BD:
OsALDH
OsPBZ1
OsPIMT1
OsPIMT2
ΔOsPIMT2
Empty
DDO
QDO
QDO/X/A
b
YFP
BF
RFP
Merge
OsPIMT1 + OsALDH
OsPIMT2 + OsALDH
ΔOsPIMT2 + OsALDH
Empty + OsALDH
OsPIMT1 + OsPBZ
OsPIMT2 + OsPBZ
ΔOsPIMT2 + OsPBZ
Empty + OsPBZ
c
Input
Pulldown
OsALDH-MBP
OsPIMT1-GST
Empty-GST
OsPBZ1-MBP
(kDa)
75
63
48
35
25
α-MBP Ab
α-GST Ab
d
IP
OsALDH-Myc
OsPBZ1-Myc
OsPIMT1-YFP
Empty-YFP
α-PIMT Ab
α-myc Ab

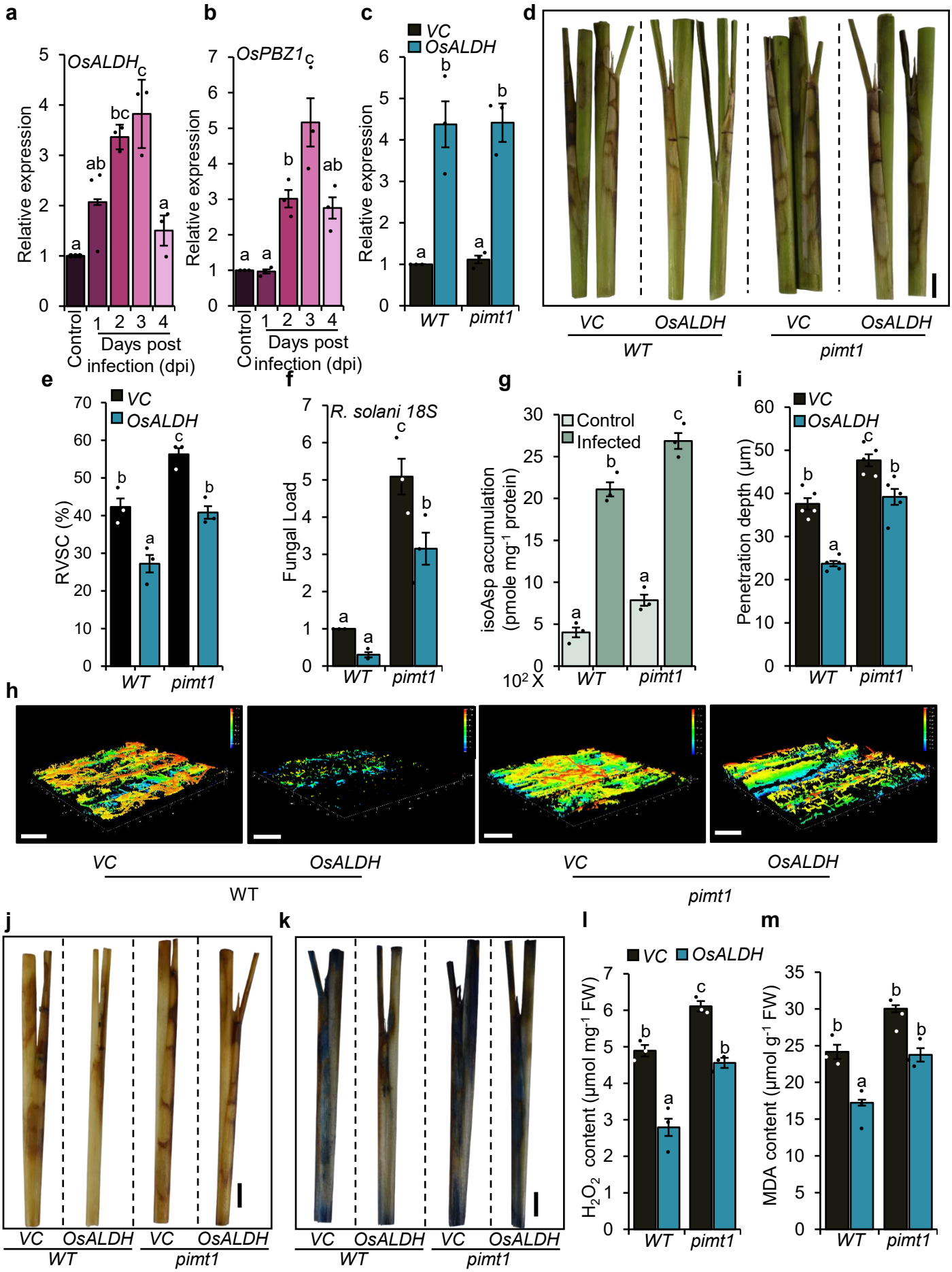
a
OsALDH
Relative expression
Control
Days post infection (dpi)
b
OsPBZ1
c
VC
OsALDH
WT
pimt1
d
e
RVSC (%)
f
R. solani 18S
Fungal Load
g
Control
Infected
isoAsp accumulation (pmole mg-1 protein)
10² X
i
Penetration depth (µm)
h
j
k
l
H2O2 content (µmol mg-1 FW)
m
MDA content (µmol g-1 FW)

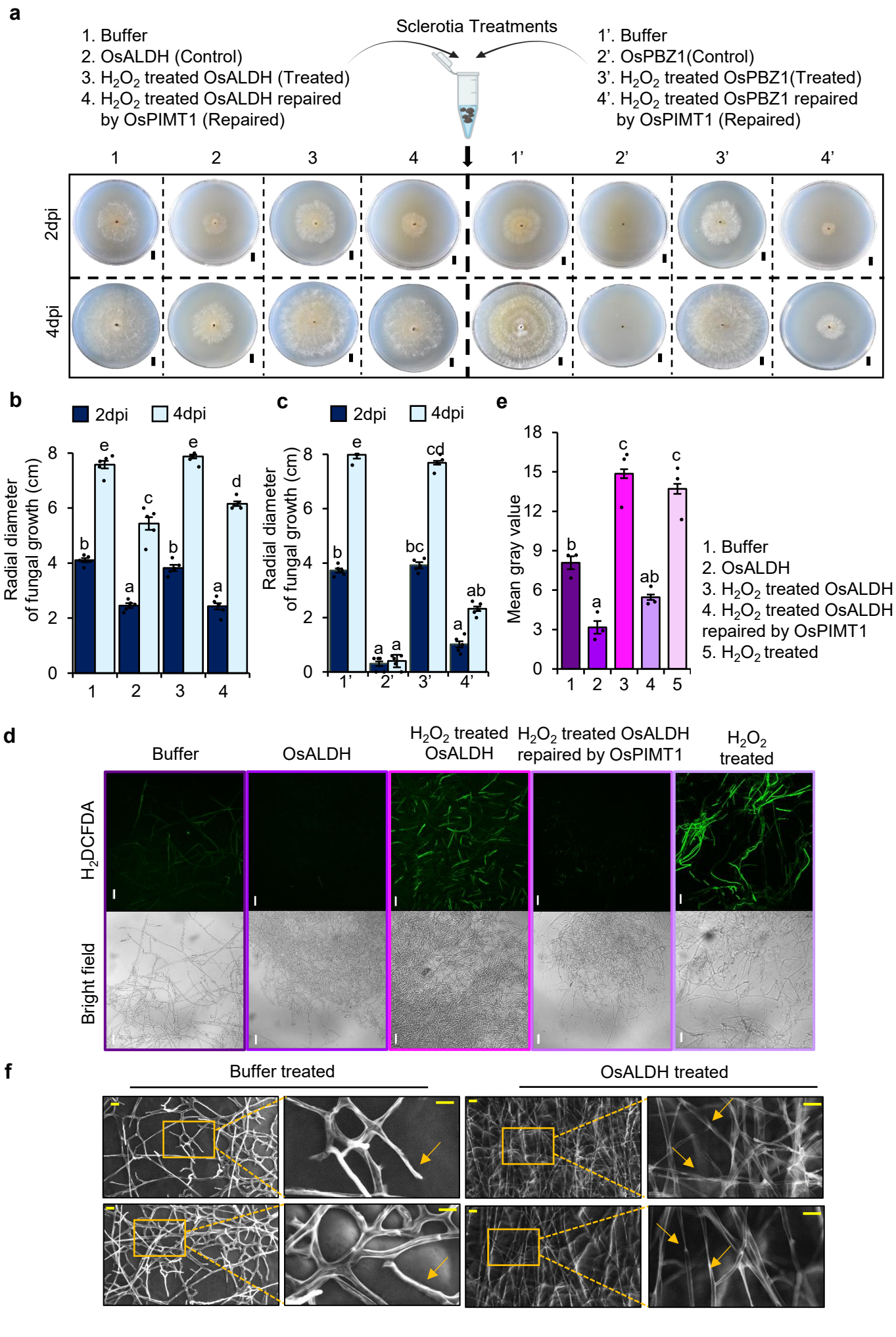
a
1. Buffer
2. OsALDH (Control)
3. H_2O_2 treated OsALDH (Treated)
4. H_2O_2 treated OsALDH repaired by OsPIMT1 (Repaired)
Sclerotia Treatments
1'. Buffer
2'. OsPBZ1(Control)
3'. H_2O_2 treated OsPBZ1(Treated)
4'. H_2O_2 treated OsPBZ1 repaired by OsPIMT1 (Repaired)
1 2 3 4 1' 2' 3' 4'
2dpi
4dpi
b
2dpi 4dpi
Radial diameter of fungal growth (cm)
1 2 3 4
c
2dpi 4dpi
Radial diameter of fungal growth (cm)
1' 2' 3' 4'
e
Mean gray value
1 2 3 4 5
1. Buffer
2. OsALDH
3. H_2O_2 treated OsALDH
4. H_2O_2 treated OsALDH repaired by OsPIMT1
5. H_2O_2 treated
d
Buffer
OsALDH
H_2O_2 treated OsALDH
H_2O_2 treated OsALDH repaired by OsPIMT1
H_2O_2 treated
H_2DCFDA
Bright field
f
Buffer treated
OsALDH treated

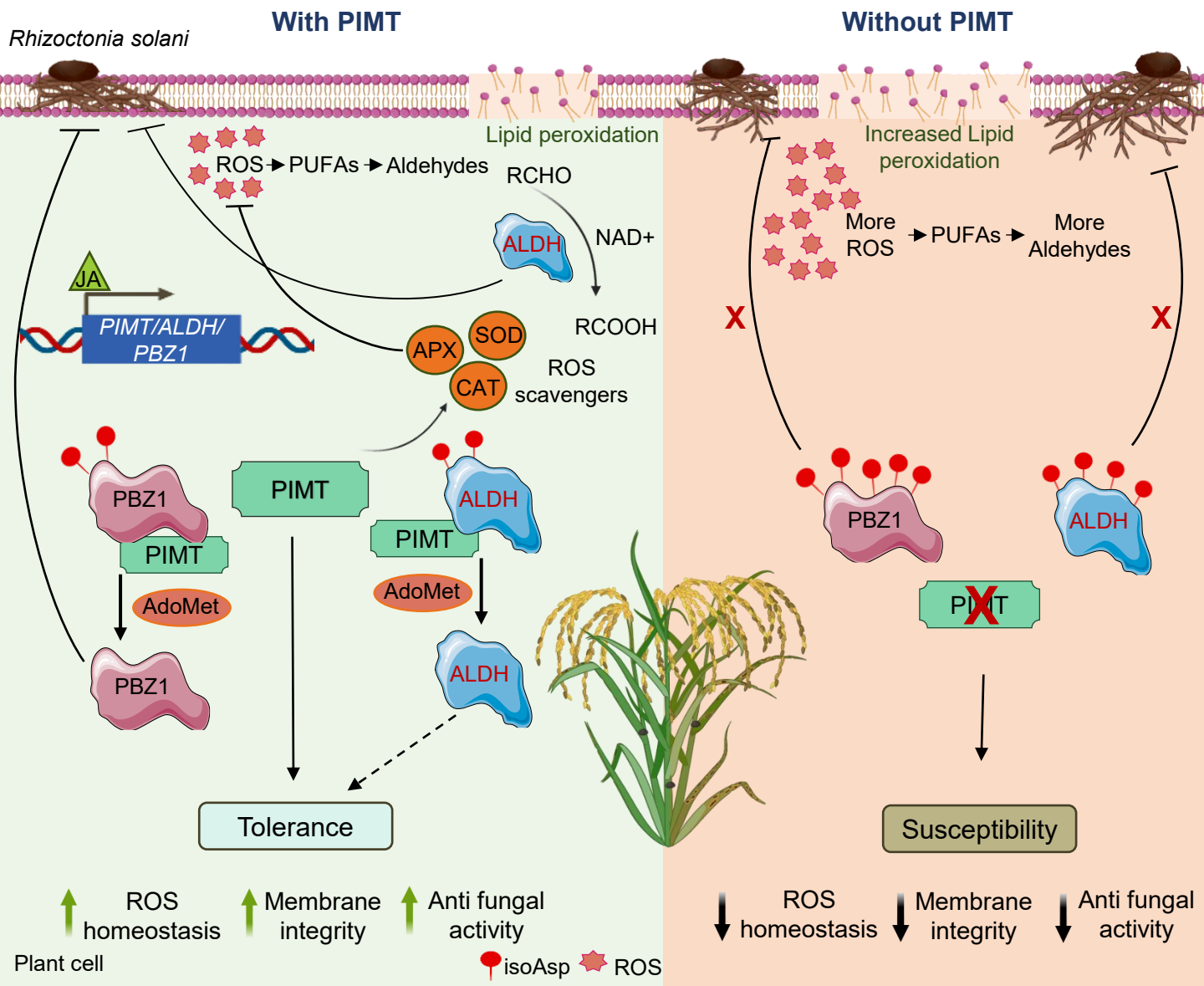
With PIMT
Without PIMT
Rhizoctonia solani
Lipid peroxidation
Increased Lipid peroxidation
ROS → PUFAs → Aldehydes
RCHO
NAD+
RCOOH
ALDH
JA
PIMT/ALDH/ PBZ1
APX
SOD
CAT
ROS scavengers
More ROS → PUFAs → More Aldehydes
X
PBZ1
PIMT
AdoMet
ALDH
Tolerance
Susceptibility
ROS homeostasis
Membrane integrity
Anti fungal activity
Plant cell
isoAsp
ROS